THE JOURNAL OF PHYSICAL CHEMISTRY C
A JOURNAL OF THE AMERICAN CHEMICAL SOCIETY

pubs.acs.org/JPCC

Review Article

Advances in Clayff Molecular Simulation of Layered and Nanoporous Materials and Their Aqueous Interfaces

Randall T. Cygan, Jeffery A. Greathouse,* and Andrey G. Kalinichev

Cite This: *J. Phys. Chem. C* 2021, 125, 17573–17589

Read Online

ACCESS | Metrics & More | Article Recommendations | Supporting Information

ABSTRACT: As a general-purpose force field for molecular simulations of layered materials and their fluid interfaces, Clayff continues to see broad usage in atomistic computational modeling for numerous geoscience and materials science applications due to its (1) success in predicting properties of bulk nanoporous materials and their interfaces, (2) transferability to a range of layered and nanoporous materials, and (3) simple functional form which facilitates incorporation into a variety of simulation codes. Here, we review applications of Clayff to model bulk phases and interfaces not included in the original parameter set and recent modifications for modeling surface terminations such as hydroxylated nanoparticle edges. We conclude with a discussion of expectations for future developments.

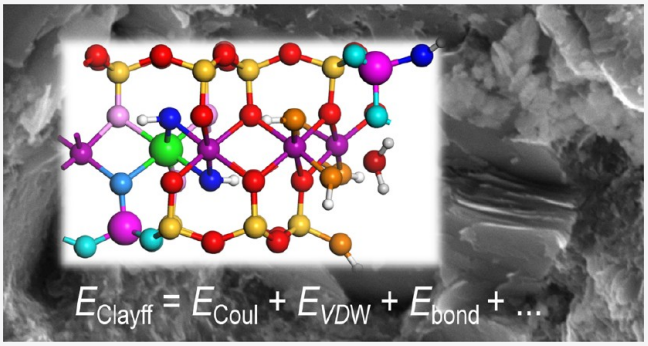

1. INTRODUCTION

Among the most innovative advances in physical chemistry over the last 50 years has been the development of molecular models for evaluating the structure, properties, dynamics, and behavior of chemical systems.[1,2] Not only have computational molecular simulation methods—including quantum-based approaches such as molecular orbital theory and density functional theory (DFT) and classical-based energy force fields—been successfully used to investigate molecules or molecular clusters, they have also been very effective in providing accurate models of layered inorganic materials, including clay minerals. The first research articles involving atomic simulations of clay minerals were published over 30 years ago,[3−5] and this specialized area of research has greatly expanded with advances in computational power and the availability of user-friendly software.

Clay minerals are layered hydrated aluminosilicates comprised of coordinated tetrahedral (T) silica sheets and octahedral (O) alumina sheets. These basic sheets are combined into TO and TOT layers, often with hydroxylated or hydrated interlayer regions. These layers stack to form nanoparticle platelets with dimensions on the order of hundreds of nanometers or a few microns for synthetic and natural samples, respectively. Layer charge can occur by substitution of Al^{3+} (or Fe^{3+}) for the tetrahedral Si^{4+} or Mg^{2+} (or Li^{+}) for octahedral Al^{3+} which results in negatively charged clay layers with charge-balancing hydrated cations, like Na^{+} and Ca^{2+}, occurring in the interlayer. Depending on the net layer charge, TOT layers can swell in aqueous environments, resulting in nanoconfined fluids relevant to numerous environmental and industrial processes. Swelling clay minerals, known collectively as smectites, include Na-montmorillonite (idealized formula $Na_{0.5}(Al_{1.5}Mg_{0.5})Si_4O_{10}(OH)_2{\cdot}nH_2O$) being one of the most common phyllosilicates. Figure 1 provides an example of Na-montmorillonite (Figure 1a), along with other layered or nanoporous materials, that can be accurately modeled using Clayff potentials.

Kaolinite, $Al_2Si_2O_5(OH)_4$, is a non-swelling TO clay mineral having no layer charge but an interlayer characterized by hydrogen bonding of hydroxyl groups between the alumina O sheet and the basal oxygens of the silica T sheet, to form TO−TO layers (Figure 1b). Many other clay minerals can be found in soils and sediments across many geological and environmental conditions and can be classified by elemental composition, layer structure, layer charge, and morphology. Layered double hydroxides (LDHs), also known as "anionic clays", which will be discussed briefly in this Review, are similar to smectite clay minerals but have hydroxylated octahedral O sheets with structural cationic substitutions that result in positive layer charge and an interlayer region with hydrated anions (e.g., Cl^{-}, CO_3^{2-}) rather than cations. Hydrotalcite, $Mg_6Al_2(OH)_{16}CO_3{\cdot}n(H_2O)$, is a representative of the LDH type of clay minerals (Figure 1c).

Because of the necessary large size of the simulation cells for many clay mineral systems, the number of atoms required for an accurate simulation ranges from many hundreds to several

Received: May 25, 2021
Revised: June 29, 2021
Published: July 22, 2021

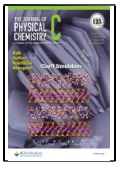

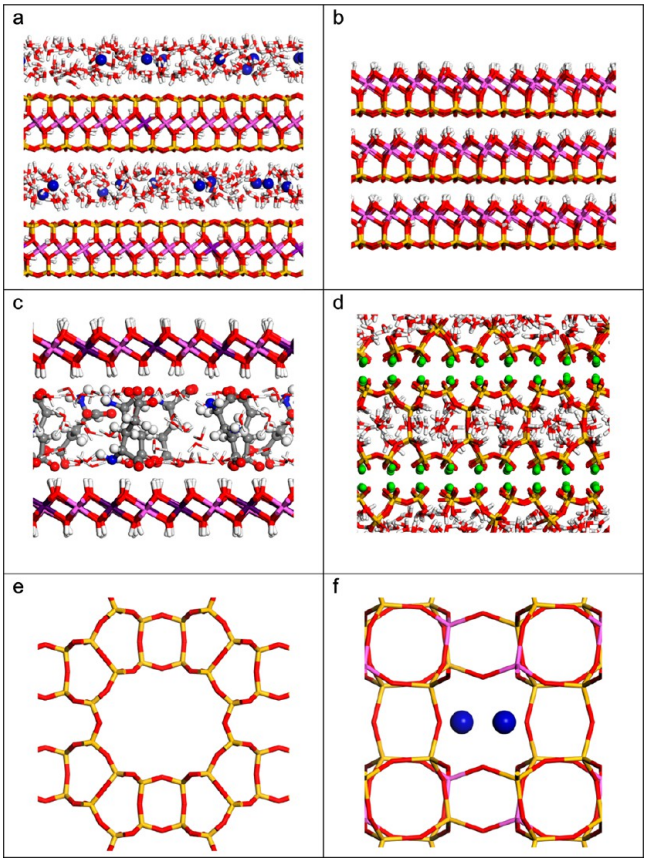

Figure 1. Models of layered and other phases that can be simulated using Clayff: (a) Na-montmorillonite (TOT clay mineral); (b) kaolinite (TO clay mineral); (c) hydrotalcite (LDH) with interlayer gluconate; (d) tobermorite, basis for the calcium silicate hydrate model (C−S−H); (e) endmember mordenite (zeolite); (f) K-feldspar (framework aluminosilicate).

millions in order to properly capture the unique composition, morphology, edge structure, and interlayer chemistry. Although quantum-based simulation methods have become relatively common among computational chemists for investigating clay mineral structures and their reactivity, computational resources continue to limit the number of atoms that can be incorporated in such intensive electronic-structure-based simulations and the time scales of the dynamic processes that can be studied by such methods. Therefore, the practitioner typically relies on a set of empirically derived interatomic potentials to accurately evaluate the interactions among the constituent atoms in the computer model.

A variety of interatomic potentials suitable for modeling clay minerals are found in the literature, and they typically involve analytical expressions describing the potential energy as a function of atomic distances, angles, or other geometric parameters.[6−8] Determination of the total potential energy of the chemical system involves the summation of Coulombic (electrostatic), van der Waals (VDW), and related nonbonded interactions with contributions from explicit bonded interactions:

$$E_{\text{Total}} = E_{\text{Coul}} + E_{\text{VDW}} + E_{\text{Bond}} + \ldots \quad (1)$$

Additional potential energy terms representing hydrostatic pressure, directional stresses, electric fields, and other intensive conditions can be incorporated. This summation would also include any interlayer ions and water molecules associated with the layered material or interface.

As an example of a standard energy calculation for a material, the computer would evaluate the Coulombic interaction energy for all atoms with each other based on their partial charge assignments, which are typically part of the force field. Dispersive or VDW interactions, which are most effective at small atomic distances, would be similarly summed. Explicitly bonded components such as hydroxyl groups and interlayer water molecules would contribute a destabilizing energy based on their deviation from equilibrium bond distances and bond angles. Validation and accuracy of these force fields—as collections of interatomic potentials are commonly referred to—will depend on the quality of the structural data, physical properties, spectroscopic data, and quantum chemical methods used to derive the best fit of the empirical parameters for each interatomic potential of the force field.

2. ORIGINS OF CLAYFF

Clayff[9] was originally developed to provide a simple and straightforward set of potentials based primarily on the nonbonded potentials described by E_{Coul} (eq 2) and E_{VDW} (eq 3)

$$E_{\text{Coul}} = \frac{e^2}{4\pi\epsilon_o} \sum_{i \neq j} \frac{q_i q_j}{r_{ij}} \quad (2)$$

where e is the fundamental charge of an electron, q_i and q_j are partial atomic charges, and r_{ij} is the distance between atoms i and j. A set of optimal and consistent values of atomic charges, based on local coordination, was derived for Clayff using electron density distributions obtained from DFT for experimental unit cell structures of a number of well-characterized simple metal oxides and hydroxides and for various molecular clusters involving hydrated metal ions. Bond stretch and three-body angle bends are also incorporated in Clayff to describe the potential energy E_{Bond} associated with explicit bonds, such as those of water molecules and hydroxyl groups.

A Lennard-Jones (L-J) potential, used to represent E_{VDW}, combines the short-range repulsion associated with atom-atom overlap and the short-range attraction associated with electron dispersion

$$E_{\text{VDW}} = \sum_{i \neq j} 4\varepsilon_{ij} \left[\left(\frac{\sigma_{ij}}{r_{ij}} \right)^{12} - \left(\frac{\sigma_{ij}}{r_{ij}} \right)^{6} \right] \quad (3)$$

where ε_{ij} is the depth of the potential energy well and σ_{ij} is the zero-crossing distance for the energy. ε_{ij} and σ_{ij} are treated as fitting parameters for the interactions between atoms i and j. For simplicity, L-J parameters in Clayff are presented for interactions between identical atom types ($i = j$), known as diagonal terms. Interaction parameters between different atom types ($i \neq j$), referred to as off-diagonal terms, are obtained using a combination of arithmetic and geometric (Lorentz-Berthelot) combining rules:[6]

$$\sigma_{ij} = \frac{\sigma_i + \sigma_j}{2} \qquad \varepsilon_{ij} = (\varepsilon_i \varepsilon_j)^{1/2} \quad (4)$$

Examples of Clayff atom types for clay minerals and edges are shown in Figure 2.

Fundamental to the parametrization of Clayff potentials is the use of equivalent VDW parameters for all oxygen atoms based on the L-J parameters for the oxygen atom of the SPC (simple

https://doi.org/10.1021/acs.jpcc.1c04600
J. Phys. Chem. C 2021, 125, 17573−17589

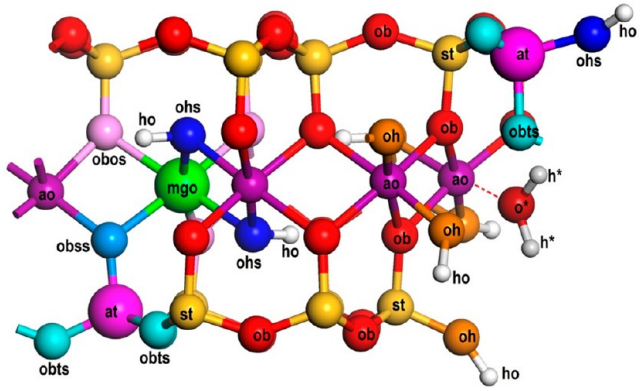

Figure 2. A fragment of a montmorillonite model with atom type parametrization according to Clayff. The complete list of atom types and their parameters is presented in Table S1. The (110) edge of the montmorillonite TOT layer is depicted on the right of the model.

point charge) water model.[10] This approach suggests that VDW parameters are the same for all clay oxygens including framework and edge oxygens, hydroxyl oxygens, and, of course, water oxygens. Only the atomic charges of these various oxygen types are different, dependent on the local bonding and coordination environment. Bond stretches associated with water molecules and hydroxyl groups are represented in Clayff by a harmonic potential where potential energy contributions increase as the square of the deviation of the bond length from its equilibrium value. Alternatively, such bond stretches can be described more accurately by a Morse potential, as was done for hydroxyl bonds in serval clay minerals.[11]

Clayff has significantly contributed to improving bulk structure simulations of clay minerals and other environmental materials, and to predicting the structural and dynamical behavior of hydrated clay interlayers and interfacial systems. The success of Clayff lies in the balanced combination of functional simplicity, relative accuracy, and transferability of the original parametrization of the force field with the fitting to structural data for simple well-characterized metal oxides and hydroxides. Furthermore, Clayff parameters are consistent with standard models of water molecules and with respective models of various aqueous cations, anions, and organic species. Physical properties are well reproduced in Clayff simulations, including most second-derivative (of energy) properties such as elastic constants, bulk moduli, dielectric constants, and vibrational spectra (Figure 3).[9]

As originally designed, Clayff excels in atomistic simulations of environmental systems involving the hydration of clay minerals and related phases. Molecular simulation studies, using Clayff potentials involving clay minerals in energy and environment applications, include oil and gas extraction and the sequestration of CO_2 and radionuclides in a variety of host materials.[12−18] Additionally, Clayff has been successfully used in the simulation of materials including zeolite and glass phases that are of particular use in technological and industrial applications.[19−22]

This Review Article provides a broad summary of Clayff and its use in the analysis of clay minerals, other clay-related and nanoporous materials, and their interfaces with aqueous solutions and other important fluids. In particular, this summary addresses recent modifications and advances in the use of Clayff since it was first introduced to the scientific community almost 20 years ago. The original authors, numerous collaborators, and other researchers have combined to improve Clayff in both practical implementations and novel applications. We first present general comments on Clayff and review the improvements made to the original interatomic potentials. We also discuss recent modifications for incorporating Clayff in the simulation of clay edge sites and how to properly implement these changes in standard molecular simulation software (Supporting Information).

Clayff was originally designed to be a general force field for the simulation of clay minerals and to have full atomic flexibility in energy optimizations and molecular dynamics (MD) simulations. Implicit in this approach was that simulations would approach accurate minimum energy configurations without the need for constrained atomic motions or fixed lattice parameters. Furthermore, dynamics simulations of aqueous interfaces involving clay surfaces, including interlayer regions of clays, would properly account for conservation of energy and momentum across the interface—for example, the interactions of clay surfaces with interlayer and interfacial cations and water molecules and their impact on diffusional transport and vibrational/librational modes.

It is also noteworthy that Clayff incorporates primarily nonbonded potentials whereby most metal−oxygen interactions in the crystal structure are assumed to be quasi-ionic and described simply by a combination of Coulombic and L-J potentials. Only hydroxyls and water molecules in Clayff incorporate bond stretching and bond-angle bending terms, using either harmonic or Morse potentials. The implementation of nonbonded potentials is helpful for describing some bond-breaking and bond-forming M−O reactions which may occur at elevated temperatures, as expected in some molten and quenched glass materials involving coordination changes.[23,24] However, such reactivity of clay minerals was not an objective in the original Clayff development, especially since the parametrization of the potentials was based on room-temperature structures of the simple oxide and hydroxide phases.

There are other force fields that have been introduced for the simulation of layered minerals.[7,25−31] Some of the early efforts in developing force fields did not treat the clay framework as fully flexible and typically relied on rigid or constrained atom arrangements. Several of the force fields developed later use a bonded form of potential to describe explicit M−O bonds in the crystal structure, and thereby focus on improving vibrational properties associated with the simulation. Other force fields have incorporated polarizable bonds to better reproduce electronic structure and the charge distribution among atoms.[32−35] As discussed in detail below, several studies have chosen to make modifications to Clayff potentials to significantly improve the accuracy for one specific class of layered or nanostructured materials. In general, each force field has its own strengths and each, including Clayff, has its own imperfections. Nonetheless, caution must be exercised when software choice and convenience preclude accuracy in the selection of an energy force field for investigating a particular material system.

3. APPLICATIONS OF CLAYFF

Clayff has been cited nearly fifteen hundred times since the parameters were first published in 2004. Clayff was initially used to simulate bulk crystal phases and aqueous interfaces of layered minerals, but an inspection of citing articles reveals that it has been used for a variety of other applications,[36] including other oxide phases, mineral−organic interactions, including contaminants, hydrocarbons,[12] natural organic matter (NOM),[37,38]

https://doi.org/10.1021/acs.jpcc.1c04600
J. Phys. Chem. C 2021, 125, 17573−17589

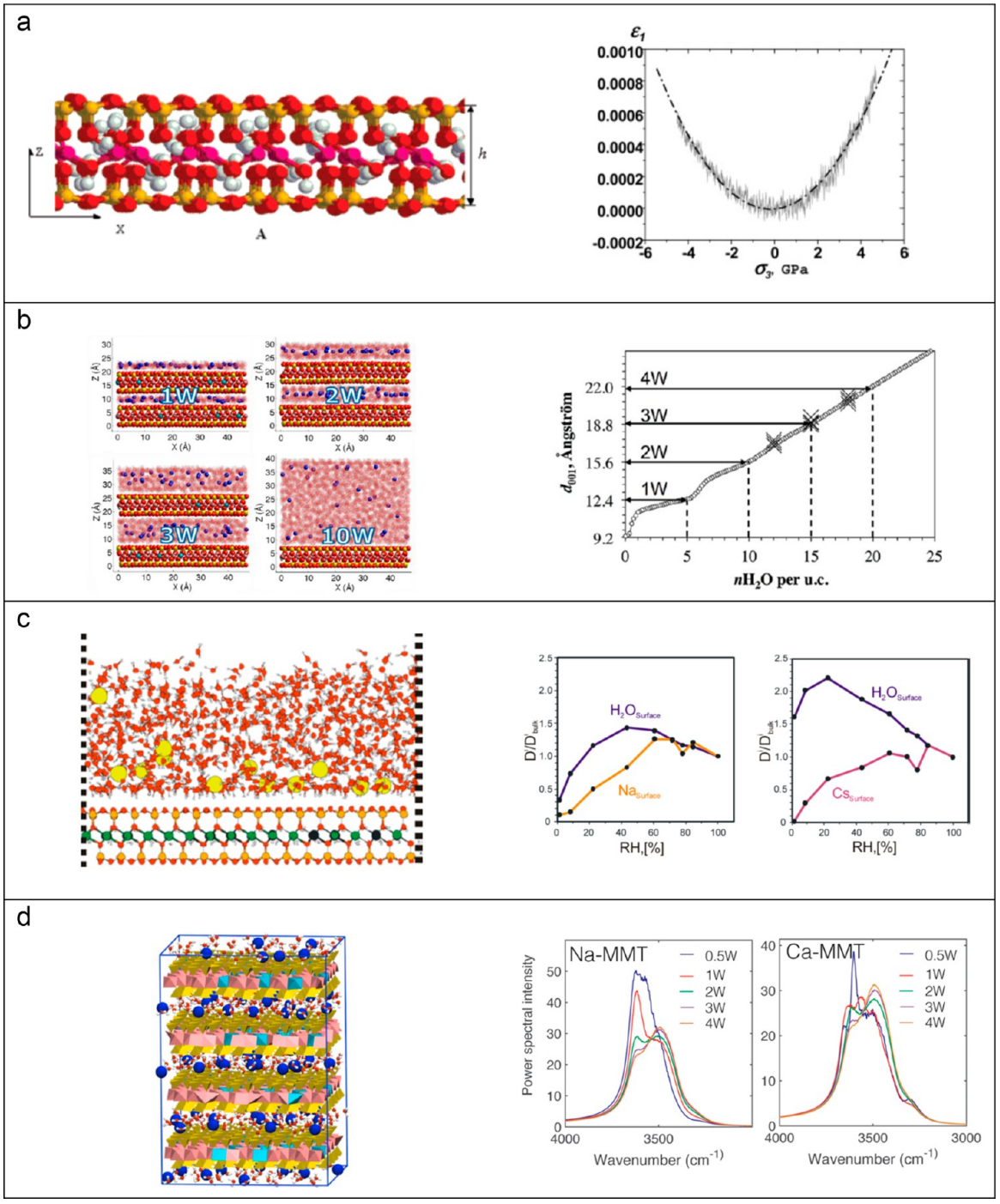

Figure 3. Material properties obtained from MD simulations using Clayff: (a) variation of pyrophyllite elastic constant under uniaxial deformation transverse to the TOT layer (z-direction);[52] (b) comparison between simulation (lines) and experiment (crosses) of basal (001) d-spacing of Na-montmorillonite with increasing water content from one water layer (1W) to four water layers (4W);[53] (c) simulated diffusion coefficients relative to bulk values for water and cations at an external surface of montmorillonite;[54] (d) simulated vibrational spectrum (O−H stretch region) of Na- and Ca-montmorillonite at different water contents.[55] Images reprinted with permission from the cited references: (a) Copyright 2008 American Chemical Society; (b) Copyright 2014 American Chemical Society; (c) Copyright 2013 American Chemical Society; (d) Copyright 2018 American Chemical Society.

biomolecules,[39−41] and polymers.[42] Clayff has also been used to model mineral phases and interfaces beyond the original training set.[43−47] Note that the following discussion is a nonexhaustive list; Clayff continues to be used and adapted into new applications. We refer the reader to previous review papers on molecular simulation of layered materials.[15,36,48−51]

Figure 3 highlights several applications using Clayff to examine the properties of clay minerals. These include simulations of the mechanical response of a montmorillonite nanoparticle,[52] the hydration and swelling behavior of Na-montmorillonite at various interlayer water contents,[53] the diffusion rates of water and cations as impacted by the clay surface,[54] and the vibrational behavior of water−siloxane

https://doi.org/10.1021/acs.jpcc.1c04600
J. Phys. Chem. C 2021, 125, 17573−17589

interactions at various water loadings of a Na-montmorillonite.[55]

3.1. Layered Silicates. Many atomistic simulations have contributed new insights to the structure and dynamics of clay minerals, their interlayers, and associated nanopores. Montmorillonite, as the most common swelling clay of the smectite mineral group, has been the subject of many of these efforts.[9,53,56−62] Successful Clayff-based models of montmorillonite have been developed to evaluate crystalline structure, hydration, interlayer structure, interlayer cation environments, swelling behavior, adsorption, and diffusion processes. Many of these efforts are related to understanding model systems for environmental applications and to advancing chemical and nuclear waste remediation and repository methods. Montmorillonite with highly expanded interlayers provides a unique model for understanding nanopores and the impact of multiple charged surfaces.

Models of kaolinite developed using Clayff potentials have also contributed to understanding TO clay structures[9,63,64] and mechanisms of cation adsorption.[65−67] Kaolinite provides two unique surface environments, where the siloxane sheet is relatively hydrophobic in contrast to the Al-octahedral sheet, which is terminated by hydroxyl groups and is hydrophilic in nature.

Even though Clayff was primarily developed for robust atomistic simulations of clay minerals and their aqueous interfaces, it was almost immediately applied to a broader range of materials, such as layered double hydroxides,[68−70] zeolites,[19] and mineral phases of cement,[43] which, similar to clay minerals, are characterized by incompletely or poorly characterized crystal structures and composition, often have large unit cells, have low symmetry, and frequently occur as only submicron size particles.[43,60,71,72] In fact, the first attempt of applying a Clayff-based approach in such simulations featured hydrocalumite (Friedel's salt), known in cement chemistry as the AFm phase.[73] The early models of layered materials, sometimes involving a few unit cells, have evolved to greater dimensions with more complex structure and chemistry. This is, in part, due to access to greater computational power but also to the simplicity of Clayff potentials and their ability to scale with system size.

3.2. Cement Phases. Over the last 10−15 years, Clayff has been successfully tested in numerous molecular simulations of cementitious materials.[43,70−72,74,75] Despite its simplicity, Clayff was proven to quite accurately reproduce the crystallographic parameters of such cement-related phases as tobermorite, ettringite, hydrocalumite, tricalcium aluminate, kanemite, and gypsum. In addition to structural properties, Clayff has been shown to reproduce quite accurately the energetics of swelling for a wide range of cement-related silicates and hydroxides.[43,74] Not unexpectedly, the MD-simulated energetics of water adsorption in Na- and K-kanemite, $[(Na,K)HSi_2O_5{\cdot}nH_2O]$, is in very good agreement with the observed X-ray diffraction, water adsorption, TGA/DTA, and ^{29}Si NMR data.[72] Kanemite-like local structures represent a realistic model of gels produced during the so-called alkali-silica-reaction (ASR) in concrete that occurs primarily due to incorporation of H_2O molecules between silicate nanoparticles, rather than within their interlayer galleries.[72]

Clayff has also been shown to well reproduce ion and water adsorption and diffusional dynamics at the surfaces of several typical cementitious materials, including hydrous calcium aluminates and the C−S−H phase represented by a tobermorite model (Figure 1d).[43,71] Good quantitative agreement between the MD-simulated diffusion coefficients of water on the surface of tobermorite, and the hopping mechanisms of longer time scale mobility of interfacial H_2O molecules, with the values obtained for hydrated cement pastes and mortars from proton field cycling NMR spin−lattice relaxation measurements, provides strong support for the molecular scale interpretation of such experimental measurements probing the behavior of water in cement nanopores.[76,77]

Even though classical approaches, such as Clayff, cannot model chemical reactions, they can still be successfully applied to simulate the systems at various equilibrium states, that is, before and after the reaction. Androniuk and Kalinichev[78] have recently applied this approach to develop a series of classical models for calcium silicate hydrates (C−S−H) corresponding to different Ca/Si ratios and different degrees of surface protonation, using experimental ^{29}Si MAS NMR data[79,80] and accurate quantum chemical results[81] as guidance. The models were then successfully applied to simulate adsorption of uranyl ions at the hydrated C−S−H surfaces as a function of Ca/Si ratio and solution pH, to determine the effects of organic molecules, such as gluconate, on these adsorption and complexation processes, and to interpret the experimentally observed behavior of these systems on a fundamental atomistic scale.[78]

3.3. Layered Double Hydroxides. Layered double hydroxides (LDHs), also known as anionic clays, represent another important class of layered materials successfully simulated using Clayff. LDHs possess positive charge in their layers and exhibit large exchange capacities for inorganic and organic anions. They have found a great variety of applications as catalysts, bio-nanocomposites and carriers for drugs, non-viral vectors for gene therapy, media for molecular separation, environmental remediation, and many other technological purposes.[82,83] The positive charge of LDH layers provides important contrast with the negative layer charges typical of aluminosilicate clay phases, which also makes LDHs useful in the investigations of the fundamental molecular scale structural and thermodynamic properties of hydrated anions in concentrated aqueous solutions.

Over the years, Clayff has been successfully applied to study the intercalation, hydration, and swelling of various LHD phases with many inorganic[70] and organic[51,68] anions (Figure 1c), including amino acids,[69,84] and even larger fragments of DNA and RNA.[85−89]

3.4. High-Charge Clay Minerals. Clayff was originally parametrized to simulate layered minerals that are either electrostatically neutral or bear a slight negative (e.g., smectite clay minerals) or slight positive (e.g., layered double hydroxides) charge. In those cases, charge delocalization predicted by quantum chemical calculations can be adequately described by smearing the net charge (± 1 e) among the four or six oxygen atoms coordinated to the substitution site. When the total layer charge is relatively low, there is little or no overlap of these smeared charges, that is, a layer oxygen atom coordinated to two charge sites. However, Clayff has also been used to simulate layered minerals with higher permanent charge, such as muscovite, saponite, vermiculite, illite, and micas. Saponite and vermiculite are swelling minerals whose interlayers expand to accommodate a few monolayers of water. Those studies have therefore focused on interlayer properties.[59,90] Illite and the mica class of clay minerals are non-swelling, so studies have been

https://doi.org/10.1021/acs.jpcc.1c04600
J. Phys. Chem. C 2021, 125, 17573−17589

limited to bulk mineral properties[91,92] or aqueous interfaces at the external basal surface.[47,57,93−98]

3.5. Layered Manganates. Phyllomanganate minerals, perhaps best represented by the hydrated phase birnessite, often control many geochemical processes involving trace and heavy element distribution in groundwater and in sediments. The high-cation exchange capacity of birnessite facilitates water purification. These phases are also important materials used in catalysis and battery applications. Birnessite has a general formula of $M_xMn_2O_4{\cdot}nH_2O$, where M is one or more hydrated interlayer cations and Mn occurs in either the tri- or tetravalent oxidation state, typically with a mean valency of +3.75. Charge analysis of manganese atoms in a geometry-optimized Na-birnessite system from DFT calculations[99] indicates a delocalization of charge for Mn consistent with the classical models of a fully occupied Na-birnessite. However, Newton and Kwon[100] suggest that some biogenic birnessites with octahedral vacancies may not exhibit such delocalization of electrons due to the vacancies.

Expanded unit cells of Na-birnessite have been used to develop and dynamically equilibrate Na-birnessite, K-birnessite, and Ba-birnessite systems to assess the structure and dynamics of interlayer water.[99] Clayff parameters for these simulations included octahedral Fe parameters (feo atom type) as a proxy for octahedral Mn in the birnessite structure. The MD simulations indicate a strong correspondence of atomic contour maps of interlayer water with observed structures obtained by synchrotron X-ray diffraction and difference electron Fourier mapping of the interlayer region (Figure 4). In particular, contour maps

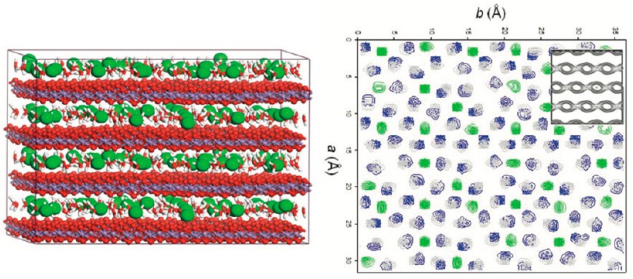

Figure 4. Simulation cell of the MD-equilibrated Na-birnessite model (left) with the corresponding density map (right) of interlayer species Na^+ (green), water oxygen (dark blue), and water hydrogen (gray).[99] The inset shows the difference electron Fourier map obtained by synchrotron X-ray diffraction and indicating positional ordering of interlayer species. Reprinted with permission from ref 99. Copyright 2012 Mineralogical Society of America.

for K-birnessite indicate diffuse regions for much of the interlayer water consistent with the low hydration enthalpy for K^+ compared to the other interlayer cations.

A recent molecular simulation study of birnessite utilizing Clayff potentials has demonstrated the role of interlayer Ni^{2+} as an electrocatalyst for water oxidation.[101] Andersen and co-workers[102] examined the adsorption of a small model protein on the basal surface of birnessite using MD simulations with Clayff to investigate the disruption of the protein structure in response to the birnessite surface. The modeling suggests the birnessite surface is more efficient at unraveling the α-helix and β-sheet structures of the protein compared to kaolinite or montmorillonite surfaces, perhaps leading to catalyzed oxidation or hydrolysis of the protein. Recent MD simulations[100,103] have used modified Clayff potentials to improve the accuracy of simulations of birnessite and related phyllomanganate structures over a range of Mn^{3+} and vacancy content. Another recent MD study[104] investigated the hydration of K-birnessite nanoparticles and successfully distinguished between intercalated (interlayer) water and externally adsorbed surface water.

Birnessite, and the previously discussed layered materials, demonstrate the versatility and robustness of Clayff molecular simulation to investigate materials that were not originally targeted in the early development of Clayff. More recent examples of the novel use of Clayff potentials to study a diverse range of materials and processes are illustrated in Figure 5.

3.6. Nanoporous Materials with Channels. Clayff was originally designed to simulate minerals with planar symmetry, but it has proven successful for nanoporous phases with one-dimensional (1D) or two-dimensional (2D) channels. Zeolites are cage-like aluminosilicate minerals consisting of 1D channels connected by cages (Figure 1e). The endmember siliceous zeolites do not bear a permanent charge, but substitution of aluminum ions at tetrahedral silicon sites results in a net negative charge. This charge is balanced by counterions. Charged zeolites readily adsorb water within the nanoscale cages, which hydrate the counterions much the same way that smectite clays expand in humid environments. The nanoscale size of zeolite cages combined with the presence of negative charge sites make zeolites extremely valuable materials for separation and catalysis applications.[111] Although unique force field parameters have been developed specifically for zeolites,[112] Clayff has also been used to model structural and dynamic properties of adsorbed species, both aqueous[19,113] and organic.[114,115] In another study, Bushuev and Sastre[21] added angle bending terms to Clayff to study the role of water in forming structural defects in a siliceous zeolite. Additionally, zeolites and fibrous clays such as palygorskite and sepiolite also contain 1D channels that are ideal environments to investigate the properties of nanoconfined water using both molecular simulation and spectroscopy.[116,117]

Clayff has also been used to simulate aluminosilicate nanotubes such as imogolite (Figure 5g) and halloysite (Figure 5h). These phases consist of TO layers similar to kaolinite, but the sheets are curved to form single walled nanotubes (imogolite) or scrolls (halloysite). The curvature of these sheets results in additional strain applied to the octahedral and tetrahedral layers, representing an acute test of Clayff parameters. Clayff has been used to study the effect of nanotube diameter on phase stability,[118] as well as the properties of water or gases at the interior and exterior walls (Figure 5g).[109,119−121]

3.7. Other Silicate Phases. Like clay minerals, the local structure of framework silicates (e.g., quartz, silica) and aluminosilicates (e.g., feldspars; Figure 1f) is dominated by tetrahedrally coordinated silicon and aluminum atoms. Not surprisingly, Clayff is well suited to simulate these structures and their fluid interfaces (Figure 5c). However, modifications to Clayff parameters (atomic charges and L-J parameters) or additional constraints (e.g., fixed atomic positions) are needed for atomic environments not included in the original force field. Many of these surfaces are terminated with hydroxyl groups, using the same harmonic O−H bond stretch term used for SPC water and layer hydroxyl groups. Kerisit and co-workers used Clayff to model orthoclase feldspar ($KAlSi_3O_8$) and forsterite (Mg_2SiO_4) and their fluid interfaces, with several modifications to Clayff for improved agreement with experimental structures.[44,45,122] Quartz and silica phases (including amorphous silica) have also been simulated using Clayff, although some

https://doi.org/10.1021/acs.jpcc.1c04600
J. Phys. Chem. C 2021, 125, 17573−17589

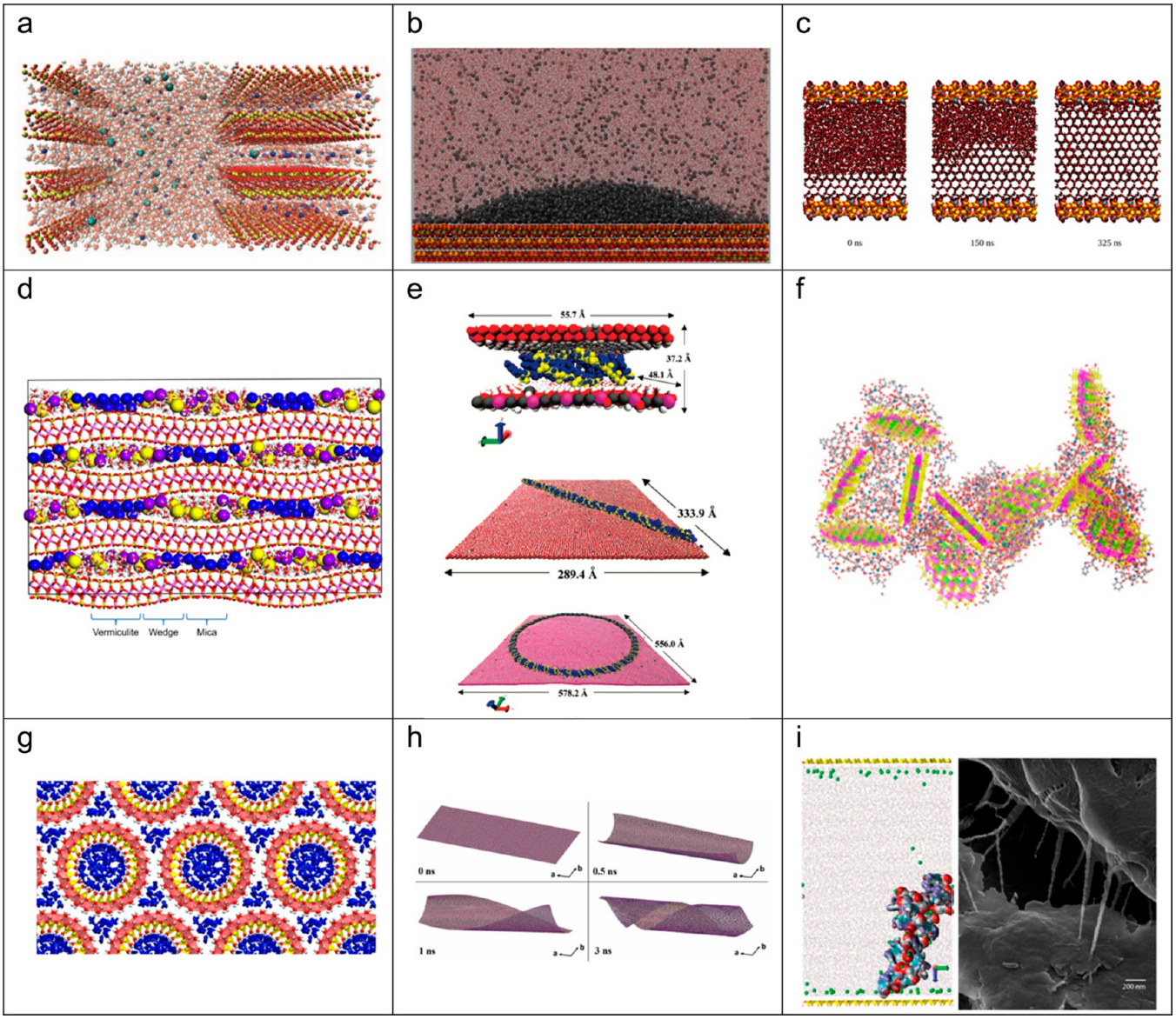

Figure 5. Selected models of layered and nanoporous phases and surfaces that have used Clayff interatomic potentials: (a) aqueous mesopore bounded by clay edges;[105] (b) supercritical CO_2 droplet in water on the siloxane surface of kaolinite;[106] (c) ice nucleation in a feldspar nanopore;[107] (d) transitional mica-vermiculite structure showing enhanced adsorption of cations;[90] (e) various types of DNA strands intercalated in LDH;[87] (f) hydrated aggregate of NOM and clay platelets;[108] (g) imogolite nanotubes saturated with water;[109] (h) evolution of kaolinite sheet into halloysite nanoribbon;[110] (i) NOM aggregate adsorbed onto a smectite nanopore with a SEM image of the natural sample.[38] Images reprinted with permission from the cited references: (a) Copyright 2016 Clay Minerals Society; (b) Copyright 2014 American Chemical Society; (c) Copyright 2019 AIP Publishing; (d) Copyright 2015 American Chemical Society; (e) Copyright 2008 American Chemical Society; (f) Copyright 2020 Elsevier; (g) Copyright 2018 American Chemical Society; (h) Copyright 2018 Royal Chemical Society; (i) Copyright 2020 American Chemical Society.

studies fixed the coordinates of silicon and oxygen atoms while allowing surface hydrogen atoms to move freely.[22,123−127]

3.8. Mesoscale Structures. Shortly after its introduction, MD simulation studies using Clayff for expanded interlayers began to appear in the literature.[66,128,129] These model systems are often referred to as external surfaces or clay nanopores,[105,130] and they serve as useful platforms to investigate the effect of fluid chemistry or pore size on adsorption and diffusion (Figures 5a and 6) and to help better understand the structure of the electric double layer (EDL). For example, Greathouse and Cygan[128] studied the effect of carbonate concentration on U(VI) adsorption onto montmorillonite surfaces, and Kerisit and Liu[122] studied the effect of pore size on water diffusion near orthoclase surfaces. Water diffusion coefficients from Clayff simulations have also been used in multiscale modeling of mesoscale clay structures.[131] Numerous Clayff studies based on nanopore models continue to be published each year for interfaces involving basal surfaces as well as hydroxylated edge surfaces. Almost all of the silica interfacial studies discussed previously used nanopore models. In recent years, such simulation studies are arguably more prevalent than those involving bulk interlayers.

3.9. Mechanical Properties. The nonbonded nature of Clayff also facilitates its use in modeling the response of layered minerals to mechanical stimuli. Fully bonded force fields usually employ rigid harmonic bond stretch and angle bending terms, resulting in more rigid layers that are less responsive to stress and strain.[26,132,133] The assumption of most bonded interactions in

https://doi.org/10.1021/acs.jpcc.1c04600
J. Phys. Chem. C 2021, 125, 17573−17589

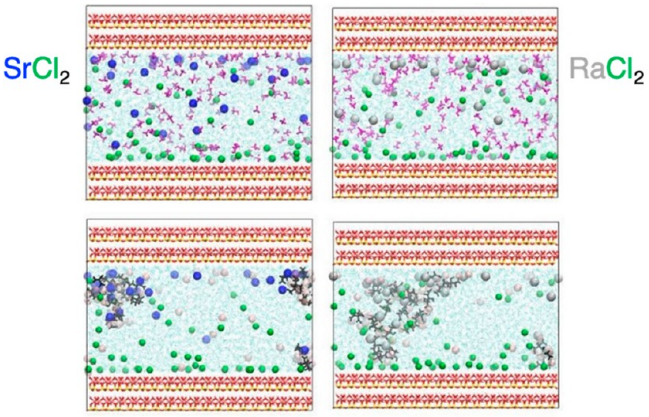

Figure 6. Snapshots of the equilibrated water-based fracturing fluids examined with methanol (top) and citric acid (bottom) additives in kaolinite mesopores, $SrCl_2$, and $RaCl_2$ salts at approximately 0.3 M concentration. Reprinted with permission from ref 67. Copyright 2018 American Chemical Society.

Clayff as quasi-ionic, using a "softer" combination of L-J interaction and electrostatic attraction, results in a more dynamic response to stress and strain. For such a simple principally nonbonded force field, Clayff gives reasonable estimates of the cleavage and surface energy of layered materials[134] but leads to less accurate estimates of elastic properties.[20,60,135]

Rutledge and co-workers were the first to investigate the mechanical properties of montmorillonite clay minerals using Clayff, initially investigating the strain dependence on vibrational frequencies[136] and then determining elastic constants of a single clay particle (Figure 3a),[52] as well as expanded clays.[137,138] Coveney and co-workers used large-scale models (more than 100,000 atoms) of montmotillonite[139] and Mg−Al LDH[140] to calculate mechanical properties including bending moduli. More recently, similar methods have been applied to investigate mechanical properties of non-swelling clays,[91] cement−graphene nanocomposites,[141] aluminosilicate nanolayers and nanotubes,[142,143] and clay−polymer nanocomposites.[144] In another application invovling second-derivative properties, Clayff was recently used for atomistic simulations of the dielectric properties of swelling clays and their dependence on water saturation and frequency.[145]

3.10. Large-Scale Moleular Simulations. Accessibility to larger and faster computational resources through massively parallel clusters and grid-exascale computing has allowed researchers to model clay mineral systems and properties that were previously considered impossible using fully atomistic simulation methods. System sizes of a few nanometers are adequate for modeling many interfacial properties such as adsorption geometries and energies, but the studies discussed below require system sizes of at least 10 nm and often simulation times of many tens of nanoseconds in order to thoroughly sample equilibrium properties. The large-scale models used by Coveney and co-workers to study the mechanical properties of clays also served to illustrate the undulatory behavior of individual clay layers.[139,140] They used similar system sizes to model polymers and biomolecules (RNA, DNA, and proteins) intercalated in clay mineral interlayers[85,87,88,146] (Figure 5e) and on mineral surfaces.[86,102] Simulations used to obtain contact angles between hydrophobic (hydrophilic) fluid phases near hydrophilic (hydrophobic) mineral surfaces require system sizes on the order of 10 nm (Figure 5b),[18,106,147] while the temperature effects on rolling of kaolinite sheets into halloysite nanotubes have been modeled at length scales up to 200 nm (Figure 5h).[110] More recently, individual clay particles consisting of single TOT layers[148] (Figure 7) or multiple TO layers[149] have been used to model the aggregation of these phases under different sedimentation environments.

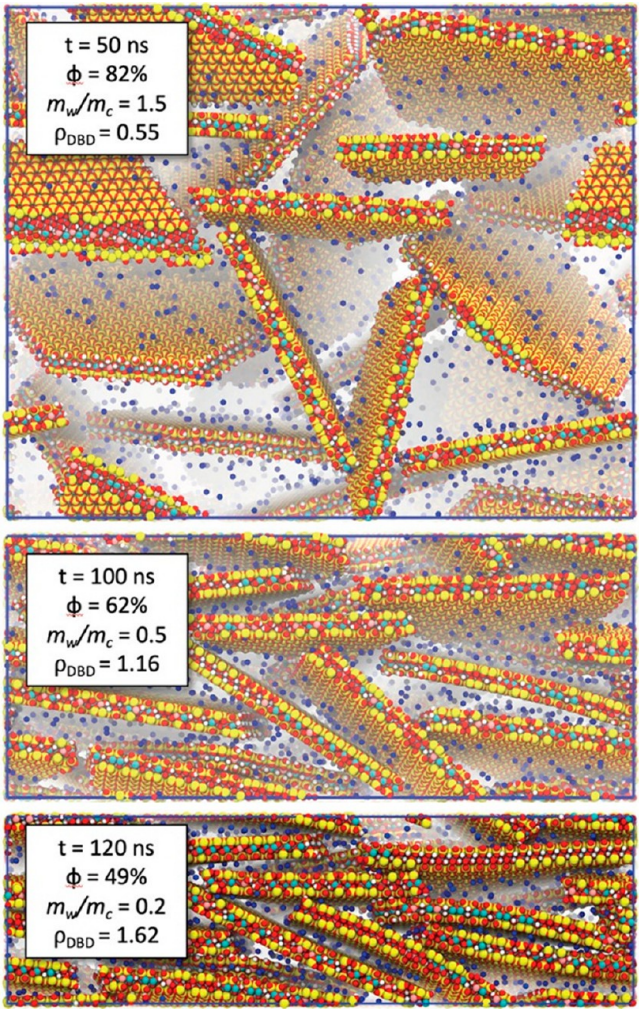

Figure 7. Snapshots of configurations predicted via MD simulation during the dehydration and compaction of a Na-montmorillonite clay suspension (water molecules not shown). The initial configuration (top) had minimal orientational correlations between clay particles, while the final structures present stacking features and correlations representative of the clay matrix. Reprinted with permission from ref 148. Copyright 2020 American Chemical Society.

4. ADVANCES IN CLAYFF

4.1. Truncated Surfaces and Edges. A systematic effort to improve Clayff parametrization is currently ongoing along two directions important in view of future application: (1) making Clayff fully compatible with more complex and more accurate models of H_2O in order to improve the accuracy of description of the structural and dynamic behavior of substrate−water interfaces and make it compatible with common force fields for organic substances;[150,151] (2) the development of additional explicit metal−O−H bending terms (Si−O−H, Al−O−H, etc.) which facilitate the accurate description of hydroxylated

https://doi.org/10.1021/acs.jpcc.1c04600
J. Phys. Chem. C 2021, 125, 17573−17589

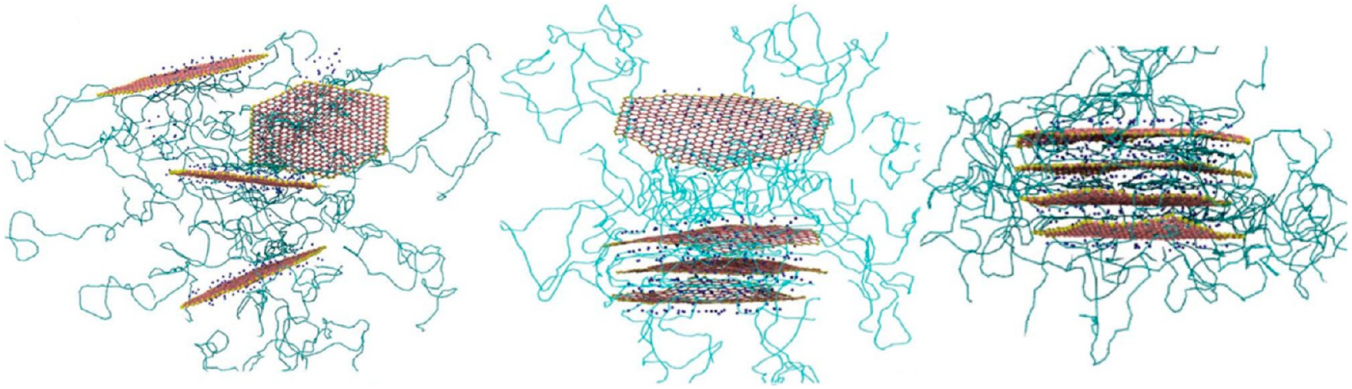

Figure 8. Snapshots from a coarse-grained MD simulation showing the intercalation of polyethylene glycol (turquoise strands) in Na-montmorillonite interlayers. Each hexagonal clay particle has lateral dimensions of approximately 100 Å. Reprinted with permission from ref 179. Copyright 2015 Wiley-VCH.

inorganic nanoparticle edges, including, for instance, the edges of C−S−H particles.[152,153]

Molecular modeling of truncated mineral surfaces presents a unique challenge for classical force fields that do not accommodate bond breaking or forming between adsorbed species and surface sites (e.g., proton transfer). The structure and net charge of hydroxylated mineral surfaces often vary with pH, which in turn affects the properties of many mineral−fluid interfaces.[154−156] The pH-dependent adsorption behavior of clay minerals is attributed to interactions at edge surfaces due to the presence of hydroxyl groups from the octahedral sheet or from dissociative water adsorption at unstable surface sites resulting from crystal growth or dissolution processes. Accurate modeling of such interfaces is needed to predict the adsorption and transport of important solute species in the subsurface.[157,158]

A growing number of studies have used Clayff to model edge surfaces of clays and other layered minerals. Typical applications include the distribution of water and solute between pore fluids and interlayers,[23,96,159−161] adsorption at edge surfaces,[16,162−164] and the simulation of nanoparticles.[148,149]

Once a molecular model for the desired edge surface is created, any dangling bonds must be repaired, typically by creating edge hydroxyl groups by adding −H (−OH) groups to MO− or M− sites, respectively. Unless surface atoms are simulated with fixed atomic position or restricted movement, these newly created edge hydroxyl groups must be simulated with additional intramolecular terms (bond stretch and/or angle bending) to prevent nonbonded hydroxyl groups from drifting into the fluid region. To accurately describe the O−H bond stretch in bulk clays or at hydroxylated surfaces, a Morse potential provides increased sensitivity to the local environment which is important when simulating vibrational properties. Morse O−H bond parameters have been developed to replace the SPC harmonic term for H_2O in Clayff.[11] However, one can still use the original SPC water harmonic term for simplicity and when the O−H bond term is not likely to affect the results (e.g., structural or transport properties at basal surfaces where layer hydroxyl groups have minimal impact on the interlayer).

Additional stability at cleaved surfaces and edges is achieved by using a three-body M−O−H angle bending term (M represents layer cations such as Al or Si). Importantly, such an angle term can be implemented while still maintaining the nonbonded pair interactions of Clayff. Parameters have been derived for cations in octahedral (Mg−O−H and Al−O−H) and tetrahedral (Si−O−H) coordination.[152,153,165] The new Clayff parametrization of the Al−O−H bending terms[152] has been recently successfully used to accurately reproduce the complex phase-sensitive vibrational sum frequency generation spectra of water on a fully hydroxylated (0001) surface of alumina.[166] Zhang and co-workers[108] have recently used the extended potentials (Pouvreau et al., 2017) of Clayff to model the interaction of soil organic matter with basal and edge surfaces of clay nanoparticles (Figure 5f and i).

The other important consideration for newly created edge surfaces is the assignment of appropriate atomic charges. Atom types for edge hydroxyl groups were not included in the original parameter set. Three approaches have been used to assign atomic charges for neutral edge surfaces: (1) use existing Clayff charges,[159,165] (2) assign new charges for hydroxyl groups and connecting atoms based on a bond valence approach,[44,96] and (3) assign charges by comparing with quantum (DFT) calculations.[163,167] In the case of octahedrally coordinated edge cations (e.g., Mg, Al), a neutral surface is obtained from original Clayff charges if one edge hydroxyl group is removed. However, physisorption of a water molecule completes the 6-fold coordination. As suggested in Figure 2, deprotonated octahedral edge sites can then be created by removing a H atom from an adsorbed water molecule and making slight adjustments, if necessary, to the hydroxyl O charge.[164]

4.2. Interlayer and Pore Fluids. Clayff has been used to simulate the interaction of many fluid and gaseous species near basal and edge surfaces. In many instances, the bulk properties of the fluid are well described by a self-consistent set of force field parameters, but interaction parameters between fluid species and mineral surfaces have not been derived for specific fluid−surface pairs. Since many force fields also use a L-J expression to describe van der Waals interactions, parameters for specific fluid−surface interactions between unlike atom types (off-diagonal parameters) can be obtained using the standard Lorentz-Berthelot combining rules (eq 4).

Clayff was originally parametrized to be consistent with the simple point charge (SPC) water model[10] using a simple harmonic approximation for the intramolecular motions.[168] However, later, its more accurate version SPC/E[169] was also successfully used.[53,59] More complex anharmonic terms can also be used to describe the bond bending and stretching terms of the structural −O−H groups and interfacial H_2O molecules for accurate simulation and interpretation of their vibrational properties.[11,151,165] There were also attempts to use a more

https://doi.org/10.1021/acs.jpcc.1c04600
J. Phys. Chem. C 2021, 125, 17573−17589

complex four-point-charge TIP4P model of H_2O[170] together with Clayff.[107,171] Improved and more accurate L-J parameters for monovalent and divalent cations compatible with SPC, SPC/E, and other water models have recently been published[172,173] and can be successfully implemented in Clayff to describe cation−water and other metal cation interactions.

Several recent studies have demonstrated a very good agreement of the 2-D and 3-D interfacial aqueous solution structures at heterogeneously charged basal and edge surfaces of clay nanoparticles simulated with Clayff with results from experimental atomic force microscopy (AFM) observations.[174−177] These studies illustrate the value of using molecular simulations as a tool in the atomistic-scale interpretation of complex AFM results.

One of the most common applications of Clayff is the simulation of organic species near mineral surfaces. Clayff was originally developed for compatibility with the consistent valence force field (CVFF),[178] which also uses the flexible SPC water model. Thus, the early Clayff simulations of mineral−organic systems combined Clayff for the surface atoms and CVFF for the organic molecules. Other mineral−organic systems have included polymers[89,138,179] and biological compounds, including constituents of amino acids and natural organic matter (Figure 5f and i).[38,68,108] Figure 8 shows stages in the polymer intercalation process from coarse-grained MD simulation.[179] This multiscale modeling approach incorporates properties from quantum calculations and Clayff simulation.

Potentials for organic compounds from the OPLS force field[180] can also be implemented with Clayff. Geoscience applications have included interlayer CO_2[181] and methane[182,183] as well as methane hydrates.[184,185] Several computational studies have investigated CO_2 and H_2O mixtures in smectite interlayers to better assess the role of carbon sequestration in mitigating climate change.[17,186,187]

In most cases, when modeling such hybrid systems, the resulting off-diagonal L-J terms governing adsorption and other nonbonded interactions have not been explicitly validated, although comparisons between Clayff-CVFF and quantum chemical methods have been made.[65] Off-diagonal parameters have been derived for specific interfaces,[163,188] but this involves a great deal of quantum chemical calculations and fitting. Nonetheless, when combining Clayff with other general force fields or atom types, it is important to check that both force fields use the same combining rules (eq 4). It is worth noting that Heinz and co-workers have streamlined the process of developing off-diagonal parameters for modeling organic species near silicate surfaces based on the INTERFACE force field.[26]

Some researchers have modified Clayff parameters in order to fit experimental or DFT-calculated properties for specific minerals or interfaces. Kerisit and co-workers have made several adjustments to Clayff L-J parameters and partial charges to improve agreement with experiment for feldspar,[44] hematite,[189] forsterite,[45] and gibbsite.[167] Adjustments to the bridging oxygen (ob) L-J parameters have been made to improve agreement with X-ray diffraction data.[59,151] Recently, Ho et al.[190] showed that thermodynamic properties of interlayer hydration and clay swelling are quite sensitive to the L-J parameters describing the interaction of aqueous cations with bridging oxygen atoms of the surface (ob). Adjustments to a subset of Clayff parameters are usually not checked for validity with other phases in the original training set, so they are not considered to be implicitly transferable. Recently, Findley and co-workers[191] have successfully used Clayff as a basis for the development of a specifically transferable force field for predicting the adsorption and diffusional mobility of hydrocarbons and small molecules in silica zeolites.

5. FUTURE DIRECTIONS

The last 30 years have seen a rapid and continuous growth in the use of computer simulation tools to investigate the molecular structure and behavior of layered materials and their interfaces that are critical to understanding the safe treatment and long-term isolation of chemical contaminants, including radionuclides, in the environment.[157,192] The physical and chemical properties of clay minerals, in particular, suggest their significant role in controlling adsorption processes and in limiting metals and organics into natural water systems that could potentially impact the quality of drinking water. Advances in microscopy, spectroscopy, and new analytical methods have helped researchers to better evaluate the mechanisms of these complex processes; however, details derived from molecular simulations are often required to supplement these methods and, in some cases, due to the nanosized and disordered or impure nature of natural clay samples, remain the only basis for understanding such processes.

Use of the Clayff energy force field in molecular simulations of layered materials has proven to be a valuable approach in these efforts. However, there remain several unique challenges for researchers in expanding and improving the accuracy of such simulations using Clayff, or other sets of potentials. One such area is the accurate simulation of the siloxane sheet structure that comprises the basal surface of many clay minerals. Results from Clayff simulations of clay phases typically exhibit hexagonal symmetry for the ring structure of the siloxane sheet. Polarizability is not the only way to introduce asymmetry. Adding bond-angle terms and adjusting VDW sigma diameters can also induce asymmetry. Even with Al substitution for Si atoms on this sheet, as found in some smectite minerals, one would expect to reduce the symmetry of the ring to ditrigonal while collapsing the size of the ring. Cation adsorption onto the basal siloxane surface may be overestimated by the more open ring structure observed in the molecular simulations.[190] Incorporation of polarization terms in classical potentials, based on DFT calculations, has led to recent improvements in modeling the rotation and tilt of tetrahedra in the tetrahedral sheet of montmorillonite and in predicting the ditrigonal symmetry for the ring structure.[32,33,193] Nonetheless, more work is needed to properly account for ionic and electronic polarization mechanisms within the framework of Clayff potentials.

Incorporating Clayff parameters in various molecular simulation codes is a straightforward process due to the nonbonded nature of the potentials. This leads to a practical and less costly approach for MD simulations that avoids having to describe bonded atom pairs that require continuous monitoring and updating during a simulation run. Although no bond between a metal and a single oxygen is explicitly defined, the Clayff interatomic potential derives a total "bond" energy in assuming the proper coordination of oxygens about the charged metal center and calculating the "bond" energy of the cluster (e.g., SiO_4, MgO_6, etc.). As long as the interatomic potentials are accurately derived from the empirical fits based on refinements of simple oxide and hydroxide crystal structures, this approach can be efficient and practical, although less analogous to defining an explicit M−O bond.

https://doi.org/10.1021/acs.jpcc.1c04600
J. Phys. Chem. C 2021, 125, 17573−17589

Clayff was developed using a consistent set of partial charges for each atom type in the force field. Values were initially derived from quantum chemical calculations and then adjusted accordingly to accommodate substitutional schemes and the stoichiometry of simulation cells for bulk phases and to make the entire charge distribution scheme consistent with the model for H_2O molecules and aqueous species. However, simulations involving surface species (e.g., edge sites), where metal coordination changes from that of the bulk environment, can become problematic when assigning partial charges. We have summarized some of the recent work in developing new Clayff potentials for these edge sites and recognize the difficulty in maintaining universal partial charges. Future development of Clayff for such sites may help guide further work on a partial charge scheme that could be easily applied to all surface sites and help guide improved potentials for protonation−deprotonation structures.

There are additional improvements that could be made to Clayff potentials. The original parameters for the nonbonded potential terms (i.e., ε and σ of the 6−12 L-J potential) could be scaled by reducing the size of the sigma terms to be consistent with physical L-J radii. In addition, it would be beneficial to practitioners to avoid combining rules when identifying L-J parameters for specific atom−atom interactions, the off-diagonal terms. This would require reporting explicit pair-interaction parameters rather than relying on diagonal terms and combining rules. Such an approach is now easier to implement with the increased use of preprocessing scripts to prepare input files. Explicit inclusion of the off-diagonal terms would also help avoid the pitfalls in using automated software to define such interactions that often confuse the user and lead to improper simulation results. Nonetheless, in part because of convention, we continue to report nonbonded potentials in terms of single atom types (diagonal format). Simulations of organic−mineral systems (e.g., clay−polymer composites) are often limited by the lack of appropriate nonbonded potentials, thereby requiring users to arbitrarily combine Clayff potentials with general organic force fields by means of various combining rules. Such an approach requires a critical eye to properly judge the worthiness of the simulation results.

Further development of Clayff should include how best to improve bonded potentials, especially for modeling metal-hydroxyl behavior in either bulk or surface structures. Our recent work has demonstrated that angle bending potentials involving metal hydroxyls need to be customized for specific hydroxyl environments.[152,153,165] Can bulk Clayff terms be simply reparameterized for surface or interfacial structures, or do completely new potentials need to be developed? Additional development work is required to accurately model Fe−O−H and Ca−O−H potentials for clay edge environments.

Lastly, much effort has been spent by van Duin and others in the development of ReaxFF[194,195] to explicitly incorporate chemical reaction dynamics into classical atomistic simulations. Incorporation of acid−base reactions such as the protonation and deprotonation of edge sites of clay minerals, or the reaction of interlayer species, would greatly broaden the predictive capabilities of such simulations for many environmentally complex and technologically important processes. Mapping potential reaction pathways associated with the interaction of aqueous solutions and clay minerals will involve substantial quantum chemical calculations coupled with machine learning methods to develop validated parameters for ReaxFF.[196,197] Nonetheless, combining the reactivity of ReaxFF, or machine-learned potentials, with Clayff potentials would significantly improve simulation accuracy and greatly expand the general application of these predictive methods.

■ ASSOCIATED CONTENT

Supporting Information

The Supporting Information is available free of charge at https://pubs.acs.org/doi/10.1021/acs.jpcc.1c04600.

A short discussion of the theoretical basis of Clayff, including analytical expressions and parameters for interatomic potential parameters, is provided; nonbonded and bonded parameters are tabulated and include values for surface/edge sites; and sample input files with Clayff parameters are presented for several commonly used molecular simulation programs (PDF)

■ AUTHOR INFORMATION

Corresponding Author

Jeffery A. Greathouse − *Geochemistry Department, Sandia National Laboratories, Albuquerque, New Mexico 87185-0754, United States;* orcid.org/0000-0002-4247-3362; Email: jagreat@sandia.gov

Authors

Randall T. Cygan − *Geochemistry Department, Sandia National Laboratories, Albuquerque, New Mexico 87185-0754, United States;* orcid.org/0000-0003-1262-6177

Andrey G. Kalinichev − *Laboratoire SUBATECH (UMR 6457 − Institut Mines-Télécom Atlantique, Université de Nantes, CNRS/IN2P3), 44307 Nantes, France;* orcid.org/0000-0003-0743-4242

Complete contact information is available at: https://pubs.acs.org/10.1021/acs.jpcc.1c04600

Author Contributions

The manuscript was written through contributions of all authors. All authors have given approval to the final version of the manuscript.

Notes

The authors declare no competing financial interest.

Biographies

Randall T. Cygan earned his Ph.D. in geochemistry and mineralogy in 1983 from Pennsylvania State University. He recently retired as Senior Scientist from Sandia National Laboratories where he worked for over 30 years. His research interests are varied, including investigations of

mineral equilibria, chemical kinetics, adsorption and dissolution of minerals, interfacial behavior of materials, shock metamorphism, and atomistic modeling of minerals, materials, and geochemical processes. He currently holds an adjunct position at Texas A&M University.

Jeffery A. Greathouse received his Ph.D. in 1996 from the University of California at Davis, followed by postdoctoral research at the University of California at Berkeley. He is a Principal Member of Technical Staff in the Geochemistry Department at Sandia National Laboratories, and he is currently President of the Clay Minerals Society. His research involves molecular simulation of aqueous systems, mineral−water interfaces, and nanoporous materials.

Andrey G. Kalinichev received his Ph.D. in chemical physics in 1986 at the Russian Academy of Sciences, where he subsequently headed the Physical Research Laboratory at the Institute of Experimental Mineralogy in Chernogolovka. After a series of Research Professorships at the University of Illinois at Urbana−Champaign and Michigan State University, he is currently a Director of Research at the Institut Mines-Télécom Atlantique in Nantes, France, where his research group is focused on atomistic computational modeling of materials and processes related to geological disposal of radioactive waste. He also served as President (2019−2020) of the Clay Minerals Society.

■ ACKNOWLEDGMENTS

This work was supported by the U.S. Department of Energy, Office of Science, Office of Basic Energy Sciences, Chemical Sciences, Geosciences and Biosciences Division under FWP 21-015452. Early development of Clayff was sponsored by the U.S. Nuclear Regulatory Commission to assist in the safe treatment and isolation of radioactive waste. Sandia National Laboratories is a multimission laboratory managed and operated by National Technology and Engineering Solutions of Sandia, LLC., a wholly owned subsidiary of Honeywell International, Inc., for the U.S. Department of Energy's National Nuclear Security Administration under contract DE-NA-0003525. The views and opinions expressed herein do not necessarily state or reflect those of the United States Government, any agency thereof, or any of their contractors. A.G.K. acknowledges support of the industrial chair "Storage and Disposal of Radioactive Waste" at the Institut Mines-Télécom Atlantique, funded by ANDRA, Orano, and EDF. We also acknowledge Lisa D. Sena-Carian for help in designing the cover graphic.

■ REFERENCES

(1) Leszczynski, J.; Shukla, M. K. *Practical Aspects of Computational Chemistry IV*; Springer International: New York, 2016; p 406.
(2) Woodley, S. M.; Catlow, C. R. A. High Performance Computing in the Chemistry of Materials. *Phys. Chem. Chem. Phys.* **2014**, *16*, 21001−21001.
(3) Aronowitz, S.; Coyne, L.; Lawless, J.; Rishpon, J. Quantum-Chemical Modeling of Smectite Clays. *Inorg. Chem.* **1982**, *21*, 3589−3593.
(4) Delville, A.; Laszlo, P. Simple Results on Cohesive Energies of Clays from a Monte Carlo Calculation. *New J. Chem.* **1989**, *13*, 481−491.
(5) Skipper, N. T.; Refson, K.; McConnell, J. D. C. Computer Calculation of Water-Clay Interactions Using Atomic Pair Potentials. *Clay Miner.* **1989**, *24*, 411−425.
(6) Allen, M. P.; Tildesley, D. J. *Computer Simulation of Liquids*, 2nd ed.; Oxford University Press: New York, 2017; p 626.
(7) Hill, J.-R.; Freeman, C. M.; Subramanian, L. Use of Force Fields in Materials Modeling. In *Reviews in Computational Chemistry*; Lipowitz, K. B., Boyd, D. B., Eds.; John Wiley and Sons: New York, 2000; Vol. *16*, pp 141−216.
(8) Leach, A. R. *Molecular Modelling: Principles and Applications*, 2nd ed.; Pearson Education: New York, 2009; p 768.
(9) Cygan, R. T.; Liang, J.-J.; Kalinichev, A. G. Molecular Models of Hydroxide, Oxyhydroxide, and Clay Phases and the Development of a General Force Field. *J. Phys. Chem. B* **2004**, *108*, 1255−1266.
(10) Berendsen, H. J. C.; Postma, J. P. M.; van Gunsteren, W. F.; Hermans, J. Interaction Models for Water in Relation to Protein Hydration. In *Intermolecular Forces*; Pullman, B., Ed.; D. Reidel: 1981; pp 331−342.
(11) Greathouse, J. A.; Durkin, J. S.; Larentzos, J. P.; Cygan, R. T. Implementation of a Morse Potential to Model Hydroxyl Behavior in Phyllosilicates. *J. Chem. Phys.* **2009**, *130*, 134713.
(12) Cole, D. R.; Ok, S.; Striolo, A.; Phan, A. Hydrocarbon Behavior at Nanoscale Interfaces. In *Reviews in Mineralogy and Geochemistry*; Hazen, R. M., Jones, A. P., Baross, J. A., Eds.; GeoScienceWorld: Washington, DC, 2013; Vol. *75*, pp 495−545.
(13) Ma, Z.; Ranjith, P. G. Review of Application of Molecular Dynamics Simulations in Geological Sequestration of Carbon Dioxide. *Fuel* **2019**, *255*, 115644.
(14) Pérez-Conesa, S.; Martínez, J. M.; Marcos, E. S. Hydration and Diffusion Mechanism of Uranyl in Montmorillonite Clay: Molecular Dynamics Using an Ab Initio Potential. *J. Phys. Chem. C* **2017**, *121*, 27437−27444.
(15) Anderson, R. L.; Ratcliffe, I.; Greenwell, H. C.; Williams, P. A.; Cliffe, S.; Coveney, P. V. Clay Swelling—A Challenge in the Oilfield. *Earth-Sci. Rev.* **2010**, *98*, 201−216.
(16) Willemsen, J. A. R.; Myneni, S. C. B.; Bourg, I. C. Molecular Dynamics Simulations of the Adsorption of Phthalate Esters on Smectite Clay Surfaces. *J. Phys. Chem. C* **2019**, *123*, 13624−13636.
(17) Myshakin, E. M.; Al-Saidi, W. A.; Romanov, V. N.; Cygan, R. T.; Jordan, K. D. Molecular Dynamics Simulations of Carbon Dioxide

https://doi.org/10.1021/acs.jpcc.1c04600
J. Phys. Chem. C 2021, 125, 17573−17589

Intercalation in Hydrated Na-Montmorillonite. *J. Phys. Chem. C* **2013**, *117*, 11028−11039.
(18) Tenney, C. M.; Dewers, T.; Chaudhary, K.; Matteo, E. N.; Cardenas, M. B.; Cygan, R. T. Experimental and Simulation Study of Carbon Dioxide, Brine, and Muscovite Surface Interactions. *J. Pet. Sci. Eng.* **2017**, *155*, 78−88.
(19) Ockwig, N. W.; Cygan, R. T.; Criscenti, L. J.; Nenoff, T. M. Molecular Dynamics Studies of Nanoconfined Water in Clinoptilolite and Heulandite Zeolites. *Phys. Chem. Chem. Phys.* **2008**, *10*, 800−807.
(20) Rimsza, J. M.; Jones, R. E.; Criscenti, L. J. Surface Structure and Stability of Partially Hydroxylated Silica Surfaces. *Langmuir* **2017**, *33*, 3882−3891.
(21) Bushuev, Y. G.; Sastre, G. Atomistic Simulations of Structural Defects and Water Occluded in SSZ-74 Zeolite. *J. Phys. Chem. C* **2009**, *113*, 10877−10886.
(22) Leroch, S.; Wendland, M. Simulation of Forces between Humid Amorphous Silica Surfaces: A Comparison of Empirical Atomistic Force Fields. *J. Phys. Chem. C* **2012**, *116*, 26247−26261.
(23) Newton, A. G.; Lee, J. Y.; Kwon, K. D. Na-Montmorillonite Edge Structure and Surface Complexes: An Atomistic Perspective. *Minerals* **2017**, *7*, 78.
(24) Tischendorf, B. C.; Alam, T. M.; Cygan, R. T.; Otaigbe, J. U. The Structure and Properties of Binary Zinc Phosphate Glasses Studied by Molecular Dynamics Simulations. *J. Non-Cryst. Solids* **2003**, *316*, 261−272.
(25) Bougeard, D.; Smirnov, K. S.; Geidel, E. Vibrational Spectra and Structure of Kaolinite: A Computer Simulation Study. *J. Phys. Chem. B* **2000**, *104*, 9210−9217.
(26) Heinz, H.; Lin, T.-J.; Mishra, R. K.; Emami, F. S. Thermodynamically Consistent Force Fields for the Assembly of Inorganic, Organic, and Biological Nanostructures: The INTERFACE Force Field. *Langmuir* **2013**, *29*, 1754−1765.
(27) Sainz-Díaz, C. I.; Hernández-Laguna, A.; Dove, M. T. Modeling of Dioctahedral 2:1 Phyllosilicates by Means of Transferable Empirical Potentials. *Phys. Chem. Miner.* **2001**, *28*, 130−141.
(28) Teppen, B. J.; Rasmussen, K.; Bertsch, P. M.; Miller, D. M.; Schäfer, L. Molecular Dynamics Modeling of Clay Minerals. 1. Gibbsite, Kaolinite, Pyrophyllite, and Beidellite. *J. Phys. Chem. B* **1997**, *101*, 1579−1587.
(29) Skipper, N. T.; Chang, F.-R. C.; Sposito, G. Monte Carlo Simulation of Interlayer Molecular Structure in Swelling Clay Minerals. 1. Methodology. *Clays Clay Miner.* **1995**, *43*, 285−293.
(30) Smith, D. E. Molecular Computer Simulations of the Swelling Properties and Interlayer Structure of Cesium Montmorillonite. *Langmuir* **1998**, *14*, 5959−5967.
(31) Kawamura, K.; Ichikawa, Y. Physical Properties of Clay Minerals and Water: By Means Molecular Dynamics Simulations. *Bull. Earthquake Res. Inst.* **2001**, *76*, 311−320.
(32) Tesson, S.; Louisfrema, W.; Salanne, M.; Boutin, A.; Ferrage, E.; Rotenberg, B.; Marry, V. Classical Polarizable Force Field to Study Hydrated Charged Clays and Zeolites. *J. Phys. Chem. C* **2018**, *122*, 24690−24704.
(33) Tesson, S.; Louisfrema, W.; Salanne, M.; Boutin, A.; Rotenberg, B.; Marry, V. Classical Polarizable Force Field to Study Dry Charged Clays and Zeolites. *J. Phys. Chem. C* **2017**, *121*, 9833−9846.
(34) Hocker, S.; Beck, P.; Schmauder, S.; Roth, J.; Trebin, H. R. Simulation of Crack Propagation in Alumina with *Ab Initio* Based Polarizable Force Field. *J. Chem. Phys.* **2012**, *136*, 084707.
(35) Brommer, P.; Beck, P.; Chatzopoulos, A.; Gähler, F.; Roth, J.; Trebin, H. R. Direct Wolf Summation of a Polarizable Force Field for Silica. *J. Chem. Phys.* **2010**, *132*, 194109.
(36) Geysermans, P.; Noguera, C. Advances in Atomistic Simulations of Mineral Surfaces. *J. Mater. Chem.* **2009**, *19*, 7807−7821.
(37) Greathouse, J. A.; Johnson, K. L.; Greenwell, H. C. Interaction of Natural Organic Matter with Layered Minerals: Recent Developments in Computational Methods at the Nanoscale. *Minerals* **2014**, *4*, 519−540.
(38) Loganathan, N.; Ferguson, B. O.; Arey, B.; Argersinger, H. E.; Bowers, G. M. A Mechanistic Exploration of Natural Organic Matter Aggregation and Surface Complexation in Smectite Mesopores. *J. Phys. Chem. A* **2020**, *124*, 9832−9843.
(39) Harding, J. H.; Duffy, D. M.; Sushko, M. L.; Rodger, P. M.; Quigley, D.; Elliott, J. A. Computational Techniques at the Organic-Inorganic Interface in Biomineralization. *Chem. Rev.* **2008**, *108*, 4823−4854.
(40) Heinz, H.; Ramezani-Dakhel, H. Simulations of Inorganic-Bioorganic Interfaces to Discover New Materials: Insights, Comparisons to Experiment, Challenges, and Opportunities. *Chem. Soc. Rev.* **2016**, *45*, 412−448.
(41) Ozboyaci, M.; Kokh, D. B.; Corni, S.; Wade, R. C. Modeling and Simulation of Protein-Surface Interactions: Achievements and Challenges. *Q. Rev. Biophys.* **2016**, *49*, 1−45.
(42) Chen, B.; Evans, J. R. G.; Greenwell, H. C.; Boulet, P.; Coveney, P. V.; Bowden, A. A.; Whiting, A. A Critical Appraisal of Polymer-Clay Nanocomposites. *Chem. Soc. Rev.* **2008**, *37*, 568−594.
(43) Kalinichev, A. G.; Wang, J. W.; Kirkpatrick, R. J. Molecular Dynamics Modeling of the Structure, Dynamics and Energetics of Mineral-Water Interfaces: Application to Cement Materials. *Cem. Concr. Res.* **2007**, *37*, 337−347.
(44) Kerisit, S.; Liu, C.; Ilton, E. S. Molecular Dynamics Simulations of the Orthoclase (001)- and (010)-Water Interfaces. *Geochim. Cosmochim. Acta* **2008**, *72*, 1481−1497.
(45) Kerisit, S.; Weare, J. H.; Felmy, A. R. Structure and Dynamics of Forsterite-scCO_2/H_2O Interfaces as a Function of Water Content. *Geochim. Cosmochim. Acta* **2012**, *84*, 137−151.
(46) Wang, J.; Kalinichev, A. G.; Kirkpatrick, R. J. Molecular Modeling of the 10-Å Phase at Subduction Zone Conditions. *Earth Planet. Sci. Lett.* **2004**, *222*, 517−522.
(47) Wang, J.; Kalinichev, A. G.; Kirkpatrick, R. J. Structure and Decompression Melting of a Novel, High-Pressure Nanoconfined 2-D Ice. *J. Phys. Chem. B* **2005**, *109*, 14308−14313.
(48) Cygan, R. T.; Greathouse, J. A.; Heinz, H.; Kalinichev, A. G. Molecular Models and Simulations of Layered Materials. *J. Mater. Chem.* **2009**, *19*, 2470−2481.
(49) Ferrage, E. Investigation of the Interlayer Organization of Water and Ions in Smectite from the Combined Use of Diffraction Experiments and Molecular Simulations. A Review of Methodology, Applications, and Perspectives. *Clays Clay Miner.* **2016**, *64*, 348−373.
(50) Greathouse, J. A.; Cygan, R. T. Molecular Simulation of Clay Minerals. In *Handbook of Clay Science*, 2nd ed.; Bergaya, F., Lagaly, G., Eds.; Elsevier: Amsterdam, The Netherlands, 2013; Vol. 5, pp 405−423.
(51) Greenwell, H. C.; Jones, W.; Coveney, P. V.; Stackhouse, S. On the Application of Computer Simulation Techniques to Anionic and Cationic Clays: A Materials Chemistry Perspective. *J. Mater. Chem.* **2006**, *16*, 708−723.
(52) Mazo, M. A.; Manevitch, L. I.; Gusarova, E. B.; Shamaev, M. Y.; Berlin, A. A.; Balabaev, N. K.; Rutledge, G. C. Molecular Dynamics Simulation of Thermomechanical Properties of Montmorillonite Crystal. 1. Isolated Clay Nanoplate. *J. Phys. Chem. B* **2008**, *112*, 2964−2969.
(53) Holmboe, M.; Bourg, I. C. Molecular Dynamics Simulations of Water and Sodium Diffusion in Smectite Interlayer Nanopores as a Function of Pore Size and Temperature. *J. Phys. Chem. C* **2014**, *118*, 1001−1013.
(54) Churakov, S. V. Mobility of Na and Cs on Montmorillonite Surface under Partially Saturated Conditions. *Environ. Sci. Technol.* **2013**, *47*, 9816−9823.
(55) Yeşilbaş, M.; Holmboe, M.; Boily, J.-F. Cohesive Vibrational and Structural Depiction of Intercalated Water in Montmorillonite. *ACS Earth Space Chem.* **2018**, *2*, 38−47.
(56) Cygan, R. T.; Daemen, L. L.; Ilgen, A. G.; Krumhansl, J. L.; Nenoff, T. M. Inelastic Neutron Scattering and Molecular Simulation of the Dynamics of Interlayer Water in Smectite Clay Minerals. *J. Phys. Chem. C* **2015**, *119*, 28005−28019.
(57) Wang, J.; Kalinichev, A. G.; Kirkpatrick, R. J. Effects of Substrate Structure and Composition on the Structure, Dynamics, and Energetics

https://doi.org/10.1021/acs.jpcc.1c04600
J. Phys. Chem. C 2021, 125, 17573−17589

of Water at Mineral Surfaces: A Molecular Dynamics Modeling Study. *Geochim. Cosmochim. Acta* **2006**, *70*, 562−582.
(58) Dazas, B.; Ferrage, E.; Delville, A.; Lanson, B. Interlayer Structure Model of Tri-Hydrated Low-Charge Smectite by X-Ray Diffraction and Monte Carlo Modeling in the Grand Canonical Ensemble. *Am. Mineral.* **2014**, *99*, 1724−1735.
(59) Ferrage, E.; Sakharov, B. A.; Michot, L. J.; Delville, A.; Bauer, A.; Lanson, B.; Grangeon, S.; Frapper, G.; Jiménez-Ruiz, M.; Cuello, G. J. Hydration Properties and Interlayer Organization of Water and Ions in Synthetic Na-Smectite with Tetrahedral Layer Charge. Part 2. Toward a Precise Coupling between Molecular Simulations and Diffraction Data. *J. Phys. Chem. C* **2011**, *115*, 1867−1881.
(60) Shahsavari, R.; Pellenq, R. J.-M.; Ulm, F.-J. Empirical Force Fields for Complex Hydrated Calcio-Silicate Layered Materials. *Phys. Chem. Chem. Phys.* **2011**, *13*, 1002−1011.
(61) Teich-McGoldrick, S. L.; Greathouse, J. A.; Jové Colón, C. F.; Cygan, R. T. Swelling Properties of Montmorillonite and Beidellite Clay Minerals from Molecular Simulation: Comparison of Temperature, Interlayer Cation, and Charge Location Effects. *J. Phys. Chem. C* **2015**, *119*, 20880−20891.
(62) Ngouana W., B. F.; Kalinichev, A. G. Structural Arrangements of Isomorphic Substitutions in Smectites: Molecular Simulation of the Swelling Properties, Interlayer Structure, and Dynamics of Hydrated Cs-Montmorillonite Revisited with New Clay Models. *J. Phys. Chem. C* **2014**, *118*, 12758−12773.
(63) Benazzouz, B. K.; Zaoui, A. Phase Diagram of Kaolinite from Molecular Dynamics Calculations. *Phys. B* **2012**, *407*, 2462−2470.
(64) Croteau, T.; Bertram, A. K.; Patey, G. N. Simulation of Water Adsorption on Kaolinite under Atmospheric Conditions. *J. Phys. Chem. A* **2009**, *113*, 7826−7833.
(65) Greathouse, J. A.; Geatches, D. L.; Pike, D. Q.; Greenwell, H. C.; Johnston, C. T.; Wilcox, J.; Cygan, R. T. Methylene Blue Adsorption on the Basal Surfaces of Kaolinite: Structure and Thermodynamics from Quantum and Classical Molecular Simulation. *Clays Clay Miner.* **2015**, *63*, 185−198.
(66) Vasconcelos, I. F.; Bunker, B. A.; Cygan, R. T. Molecular Dynamics Modeling of Ion Adsorption to the Basal Surfaces of Kaolinite. *J. Phys. Chem. C* **2007**, *111*, 6753−6762.
(67) Papavasileiou, K. D.; Michalis, V. K.; Peristeras, L. D.; Vasileiadis, M.; Striolo, A.; Economou, I. G. Molecular Dynamics Simulation of Water-Based Fracturing Fluids in Kaolinite Slit Pores. *J. Phys. Chem. C* **2018**, *122*, 17170−17183.
(68) Kumar, P. P.; Kalinichev, A. G.; Kirkpatrick, R. J. Molecular Dynamics Simulation of the Energetics and Structure of Layered Double Hydroxides Intercalated with Carboxylic Acids. *J. Phys. Chem. C* **2007**, *111*, 13517−13523.
(69) Greenwell, H. C.; Coveney, P. V. Layered Double Hydroxide Minerals as Possible Prebiotic Information Storage and Transfer Compounds. *Origins Life Evol. Biospheres* **2006**, *36*, 13−37.
(70) Kirkpatrick, R. J.; Kalinichev, A. G.; Wang, J.; Hou, X.; Amonette, J. E. Molecular Modeling of the Vibrational Spectra of Interlayer and Surface Species of Layered Double Hydroxides. In *The Application of Vibrational Spectra to Clay Minerals and Layered Double Hydroxides*; Kloprogge, J. T., Ed.; Clay Minerals Society: Aurora, CO, 2005; Vol. *13*, pp 239−285.
(71) Kalinichev, A. G.; Kirkpatrick, R. J. Molecular Dynamics Modeling of Chloride Binding to the Surfaces of Calcium Hydroxide, Hydrated Calcium Aluminate, and Calcium Silicate Phases. *Chem. Mater.* **2002**, *14*, 3539−3549.
(72) Kirkpatrick, R. J.; Kalinichev, A. G.; Hou, X.; Struble, L. Experimental and Molecular Dynamics Modeling Studies of Interlayer Swelling: Water Incorporation in Kanemite and ASR Gel. *Mater. Struct.* **2005**, *38*, 449−458.
(73) Kalinichev, A. G.; Kirkpatrick, R. J.; Cygan, R. T. Molecular Modeling of the Structure and Dynamics of the Interlayer and Surface Species of Mixed-Metal Layered Hydroxides: Chloride and Water in Hydrocalumite (Friedel's Salt). *Am. Mineral.* **2000**, *85*, 1046−1052.
(74) Kirkpatrick, R. J.; Kalinichev, A. G.; Bowers, G. M.; Yazaydin, A. Ö.; Krishnan, M.; Saharay, M.; Morrow, C. P. NMR and Computational Molecular Modeling Studies of Mineral Surfaces and Interlayer Galleries: A Review. *Am. Mineral.* **2015**, *100*, 1341−1354.
(75) Mutisya, S. M.; de Almeida, J. M.; Miranda, C. R. Molecular Simulations of Cement Based Materials: A Comparison between First Principles and Classical Force Field Calculations. *Comput. Mater. Sci.* **2017**, *138*, 392−402.
(76) Korb, J. P.; McDonald, P. J.; Monteilhet, L.; Kalinichev, A. G.; Kirkpatrick, R. J. Comparison of Proton Field-Cycling Relaxometry and Molecular Dynamics Simulations for Proton-Water Surface Dynamics in Cement-Based Materials. *Cem. Concr. Res.* **2007**, *37*, 348−350.
(77) Mishra, R. K.; et al. Cemff: A Force Field Database for Cementitious Materials Including Validations, Applications and Opportunities. *Cem. Concr. Res.* **2017**, *102*, 68−89.
(78) Androniuk, I.; Kalinichev, A. G. Molecular Dynamics Simulation of the Interaction of Uranium (VI) with the C-S-H Phase of Cement in the Presence of Gluconate. *Appl. Geochem.* **2020**, *113*, 104496.
(79) Beaudoin, J. J.; Raki, L.; Alizadeh, R. A ^{29}Si MAS NMR Study of Modified C-S-H Nanostructures. *Cem. Concr. Compos.* **2009**, *31*, 585−590.
(80) Cong, X.; Kirkpatrick, R. J. ^{29}Si MAS NMR Study of the Structure of Calcium Silicate Hydrate. *Adv. Cem. Based Mater.* **1996**, *3*, 144−156.
(81) Churakov, S. V.; Labbez, C.; Pegado, L.; Sulpizi, M. Intrinsic Acidity of Surface Sites in Calcium Silicate Hydrates and Its Implication to Their Electrokinetic Properties. *J. Phys. Chem. C* **2014**, *118*, 11752−11762.
(82) Duan, X.; Evans, D. G. *Layered Double Hydroxides*; Springer-Verlag: Berlin, 2006; Vol. *119*, p 246.
(83) Rives, V. *Layered Double Hydroxides: Present and Future*; Nova Science Publishers: New York, 2001; p 439.
(84) Kalinichev, A. G.; Kumar, P. P.; Kirkpatrick, R. J. Molecular Dynamics Computer Simulations of the Effects of Hydrogen Bonding on the Properties of Layered Double Hydroxides Intercalated with Organic Acids. *Philos. Mag.* **2010**, *90*, 2475−2488.
(85) Suter, J. L.; Coveney, P. V. Materials Properties of Clay Nanocomposites: Onset of Negative Poisson Ratio in Large-Scale Molecular Dynamics Simulation. *Soft Matter* **2009**, *5*, 3896−3904.
(86) Swadling, J. B.; Suter, J. L.; Greenwell, H. C.; Coveney, P. V. Influence of Surface Chemistry and Charge on Mineral-RNA Interactions. *Langmuir* **2013**, *29*, 1573−1583.
(87) Thyveetil, M. A.; Coveney, P. V.; Greenwell, H. C.; Suter, J. L. Computer Simulation Study of the Structural Stability and Materials Properties of DNA-Intercalated Layered Double Hydroxides. *J. Am. Chem. Soc.* **2008**, *130*, 4742−4756.
(88) Thyveetil, M. A.; Coveney, P. V.; Greenwell, H. C.; Suter, J. L. Role of Host Layer Flexibility in DNA Guest Intercalation Revealed by Computer Simulation of Layered Nanomaterials. *J. Am. Chem. Soc.* **2008**, *130*, 12485−12495.
(89) Suter, J. L.; Anderson, R. L.; Greenwell, H. C.; Coveney, P. V. Recent Advances in Large-Scale Atomistic and Coarse-Grained Molecular Dynamics Simulation of Clay Minerals. *J. Mater. Chem.* **2009**, *19*, 2482−2493.
(90) Zaunbrecher, L. K.; Cygan, R. T.; Elliott, W. C. Molecular Models of Cesium and Rubidium Adsorption on Weathered Micaceous Minerals. *J. Phys. Chem. A* **2015**, *119*, 5691−5700.
(91) Hantal, G.; Brochard, L.; Laubie, H.; Ebrahimi, D.; Pellenq, R. J. M.; Ulm, F. J.; Coasne, B. Atomic-Scale Modelling of Elastic and Failure Properties of Clays. *Mol. Phys.* **2014**, *112*, 1294−1305.
(92) Teich-McGoldrick, S. L.; Greathouse, J. A.; Cygan, R. T. Molecular Dynamics Simulations of Structural and Mechanical Properties of Muscovite: Pressure and Temperature Effects. *J. Phys. Chem. C* **2012**, *116*, 15099−15107.
(93) Adapa, S.; Swamy, D. R.; Kancharla, S.; Pradhan, S.; Malani, A. Role of Mono- and Divalent Surface Cations on the Structure and Adsorption Behavior of Water on Mica Surface. *Langmuir* **2018**, *34*, 14472−14488.
(94) Bourg, I. C.; Lee, S. S.; Fenter, P.; Tournassat, C. Stern Layer Structure and Energetics at Mica-Water Interfaces. *J. Phys. Chem. C* **2017**, *121*, 9402−9412.

(95) Fedyanin, I.; Pertsin, A.; Grunze, M. Quasistatic Computer Simulations of Shear Behavior of Water Nanoconfined between Mica Surfaces. *J. Chem. Phys.* **2011**, *135*, 174704.
(96) Lammers, L. N.; Bourg, I. C.; Okumura, M.; Kolluri, K.; Sposito, G.; Machida, M. Molecular Dynamics Simulations of Cesium Adsorption on Illite Nanoparticles. *J. Colloid Interface Sci.* **2017**, *490*, 608−620.
(97) Rahromostaqim, M.; Sahimi, M. Molecular Dynamics Simulation of Hydration and Swelling of Mixed-Layer Clays. *J. Phys. Chem. C* **2018**, *122*, 14631−14639.
(98) Wang, J.; Kalinichev, A. G.; Kirkpatrick, R. J.; Cygan, R. T. Structure, Energetics, and Dynamics of Water Adsorbed on the Muscovite (001) Surface: A Molecular Dynamics Simulation. *J. Phys. Chem. B* **2005**, *109*, 15893−15905.
(99) Cygan, R. T.; Post, J. E.; Heaney, P. J.; Kubicki, J. D. Molecular Models of Birnessite and Related Hydrated Layered Minerals. *Am. Mineral.* **2012**, *97*, 1505−1514.
(100) Newton, A. G.; Kwon, K. D. Molecular Simulations of Hydrated Phyllomanganates. *Geochim. Cosmochim. Acta* **2018**, *235*, 208−223.
(101) Thenuwara, A. C.; et al. Nickel Confined in the Interlayer Region of Birnessite: An Active Electrocatalyst for Water Oxidation. *Angew. Chem., Int. Ed.* **2016**, *55*, 10381−10385.
(102) Andersen, A.; Reardon, P. N.; Chacon, S. S.; Qafoku, N. P.; Washton, N. M.; Kleber, M. Protein-Mineral Interactions: Molecular Dynamics Simulations Capture Importance of Variations in Mineral Surface Composition and Structure. *Langmuir* **2016**, *32*, 6194−6209.
(103) Newton, A. G.; Kwon, K. D. Classical Mechanical Simulations of Layer- and Tunnel-Structured Manganese Oxide Minerals. *Geochim. Cosmochim. Acta* **2020**, *291*, 92−109.
(104) Cheng, W.; Lindholm, J.; Holmboe, M.; Luong, N. T.; Shchukarev, A.; Ilton, E. S.; Hana, K.; Boily, J.-F. Nanoscale Hydration in Layered Manganese Oxides. *Langmuir* **2021**, *37*, 666−674.
(105) Tournassat, C.; Bourg, I. C.; Holmboe, M.; Sposito, G.; Steefel, C. I. Molecular Dynamics Simulations of Anion Exclusion in Clay Interlayer Nanopores. *Clays Clay Miner.* **2016**, *64*, 374−388.
(106) Tenney, C. M.; Cygan, R. T. Molecular Simulation of Carbon Dioxide, Brine, and Clay Mineral Interactions and Determination of Contact Angles. *Environ. Sci. Technol.* **2014**, *48*, 2035−2042.
(107) Soni, A.; Patey, G. N. Simulations of Water Structure and the Possibility of Ice Nucleation on Selected Crystal Planes of K-Feldspar. *J. Chem. Phys.* **2019**, *150*, 214501.
(108) Zhang, Y.; Liu, X.; Zhang, C.; Lu, X. A Combined First Principles and Classical Molecular Dynamics Study of Clay-Soil Organic Matters (SOMs) Interactions. *Geochim. Cosmochim. Acta* **2020**, *291*, 110−125.
(109) Scalfi, L.; Fraux, G.; Boutin, A.; Coudert, F. X. Structure and Dynamics of Water Confined in Imogolite Nanotubes. *Langmuir* **2018**, *34*, 6748−6756.
(110) Prishchenko, D. A.; Zenkov, E. V.; Mazurenko, V. V.; Fakhrullin, R. F.; Lvov, Y. M.; Mazurenko, V. G. Molecular Dynamics of the Halloysite Nanotubes. *Phys. Chem. Chem. Phys.* **2018**, *20*, 5841−5849.
(111) Kulprathipanja, S. *Zeolites in Industrial Separation and Catalysis*; Wiley-VCH: Weinheim, Germany, 2010; p 593.
(112) Smit, B.; Maesen, T. L. M. Molecular Simulations of Zeolites: Adsorption, Diffusion, and Shape Selectivity. *Chem. Rev.* **2008**, *108*, 4125−4184.
(113) Ockwig, N. W.; Cygan, R. T.; Hartl, M. A.; Daemen, L. L.; Nenoff, T. M. Incoherent Inelastic Neutron Scattering Studies of Nanoconfined Water in Clinoptilolite and Heulandite Zeolites. *J. Phys. Chem. C* **2008**, *112*, 13629−13634.
(114) Narasimhan, L.; Kuchta, B.; Schaef, O.; Brunet, P.; Boulet, P. Mechanism of Adsorption of *p*-Cresol Uremic Toxin into Faujasite Zeolites in Presence of Water and Sodium Cations - A Monte Carlo Study. *Microporous Mesoporous Mater.* **2013**, *173*, 70−77.
(115) Deng, Y.; Szczerba, M. Computational Evaluation of Bonding between Aflatoxin B_1 and Smectite. *Appl. Clay Sci.* **2011**, *54*, 26−33.
(116) Ockwig, N. W.; Greathouse, J. A.; Durkin, J. S.; Cygan, R. T.; Daemen, L. L.; Nenoff, T. M. Nanoconfined Water in Magnesium-Rich 2:1 Phyllosilicates. *J. Am. Chem. Soc.* **2009**, *131*, 8155−8162.
(117) Zhou, J.; Lu, X.; Boek, E. S. Confined Water in Tunnel Nanopores of Sepiolite: Insights from Molecular Simulations. *Am. Mineral.* **2016**, *101*, 713−718.
(118) González, R. I.; Ramírez, R.; Rogan, J.; Valdivia, J. A.; Munoz, F.; Valencia, F.; Ramírez, M.; Kiwi, M. Model for Self-Rolling of an Aluminosilicate Sheet into a Single-Walled Imogolite Nanotube. *J. Phys. Chem. C* **2014**, *118*, 28227−28233.
(119) González, R. I.; et al. Imogolite in Water: Simulating the Effects of Nanotube Curvature on Structure and Dynamics. *Appl. Clay Sci.* **2020**, *191*, 105582.
(120) Presti, D.; Pedone, A.; Mancini, G.; Duce, C.; Tine, M. R.; Barone, V. Insights into Structural and Dynamical Features of Water at Halloysite Interfaces Probed by DFT and Classical Molecular Dynamics Simulations. *Phys. Chem. Chem. Phys.* **2016**, *18*, 2164−2174.
(121) Zang, J.; Chempath, S.; Konduri, S.; Nair, S.; Sholl, D. S. Flexibility of Ordered Surface Hydroxyls Influences the Adsorption of Molecules in Single-Walled Aluminosilicate Nanotubes. *J. Phys. Chem. Lett.* **2010**, *1*, 1235−1240.
(122) Kerisit, S.; Liu, C. Molecular Simulations of Water and Ion Diffusion in Nanosized Mineral Fractures. *Environ. Sci. Technol.* **2009**, *43*, 777−782.
(123) Bourg, I. C.; Steefel, C. I. Molecular Dynamics Simulations of Water Structure and Diffusion in Silica Nanopores. *J. Phys. Chem. C* **2012**, *116*, 11556−11564.
(124) Ho, T. A.; Argyris, D.; Papavassiliou, D. V.; Striolo, A.; Lee, L. L.; Cole, D. R. Interfacial Water on Crystalline Silica: A Comparative Molecular Dynamics Simulation Study. *Mol. Simul.* **2011**, *37*, 172−195.
(125) Knight, A. W.; Ilani-Kashkouli, P.; Harvey, J. A.; Greathouse, J. A.; Ho, T. A.; Kabengi, N.; Ilgen, A. G. Interfacial Reactions of Cu(II) Adsorption and Hydrolysis Driven by Nano-Scale Confinement. *Environ. Sci.: Nano* **2020**, *7*, 68−80.
(126) Kroutil, O.; Chival, Z.; Skelton, A. A.; Předota, M. Computer Simulations of Quartz (101)-Water Interface over a Range of pH Values. *J. Phys. Chem. C* **2015**, *119*, 9274−9286.
(127) Skelton, A. A.; Wesolowski, D. J.; Cummings, P. T. Investigating the Quartz $(10\bar{1}0)$/Water Interface Using Classical and Ab Initio Molecular Dynamics. *Langmuir* **2011**, *27*, 8700−8709.
(128) Greathouse, J. A.; Cygan, R. T. Molecular Dynamics Simulation of Uranyl(VI) Adsorption Equilibria onto an External Montmorillonite Surface. *Phys. Chem. Chem. Phys.* **2005**, *7*, 3580−3586.
(129) Greathouse, J. A.; Cygan, R. T. Water Structure and Aqueous Uranyl(VI) Adsorption Equilibria onto External Surfaces of Beidellite, Montmorillonite, and Pyrophyllite: Results from Molecular Simulations. *Environ. Sci. Technol.* **2006**, *40*, 3865−3871.
(130) Greathouse, J. A.; Hart, D. B.; Bowers, G. M.; Kirkpatrick, R. J.; Cygan, R. T. Molecular Simulation of Structure and Diffusion at Smectite-Water Interfaces: Using Expanded Clay Interlayers as Model Nanopores. *J. Phys. Chem. C* **2015**, *119*, 17126−17136.
(131) Churakov, S. V.; Gimmi, T. Up-Scaling of Molecular Diffusion Coefficients in Clays: A Two-Step Approach. *J. Phys. Chem. C* **2011**, *115*, 6703−6714.
(132) Sato, H.; Yamagishi, A.; Kawamura, K. Molecular Simulation for Flexibility of a Single Clay Layer. *J. Phys. Chem. B* **2001**, *105*, 7990−7997.
(133) Zartman, G. D.; Liu, H.; Akdim, B.; Pachter, R.; Heinz, H. Nanoscale Tensile, Shear, and Failure Properties of Layered Silicates as a Function of Cation Density and Stress. *J. Phys. Chem. C* **2010**, *114*, 1763−1772.
(134) Heinz, H.; Koerner, H.; Anderson, K. L.; Vaia, R. A.; Farmer, B. L. Force Field for Mica-Type Silicates and Dynamics of Octadecylammonium Chains Grafted to Montmorillonite. *Chem. Mater.* **2005**, *17*, 5658−5669.
(135) Claverie, J.; Kamali-Bernard, S.; Cordeiro, J. M. M.; Bernard, F. Assessment of Mechanical, Thermal Properties and Crystal Shapes of Monoclinic Tricalcium Silicate from Atomistic Simulations. *Cem. Concr. Res.* **2021**, *140*, 106269.

(136) Kalra, A.; Parks, D. M.; Rutledge, G. C. Molecular Simulation of Strain Dependence of Vibrational Frequencies for Montmorillonite Clay and Analysis of Strain Transfer in a Polymer-Clay Nanocomposite. *Macromolecules* **2007**, *40*, 140−144.
(137) Mazo, M. A.; Manevitch, L. I.; Gusarova, E. B.; Berlin, A. A.; Balabaev, N. K.; Rutledge, G. C. Molecular Dynamics Simulation of Thermomechanical Properties of Montmorillonite Crystal. II. Hydrated Montmorillonite Crystal. *J. Phys. Chem. C* **2008**, *112*, 17056−17062.
(138) Mazo, M. A.; Manevitch, L. I.; Gusarova, E. B.; Shamaev, M. Y.; Berlin, A. A.; Balabaev, N. K.; Rutledge, G. C. Molecular Dynamics Simulation of Thermomechanical Properties of Montmorillonite Crystal. 3. Montmorillonite Crystals with PEO Oligomer Intercalates. *J. Phys. Chem. B* **2008**, *112*, 3597−3604.
(139) Suter, J. L.; Coveney, P. V.; Greenwell, H. C.; Thyveetil, M. A. Large-Scale Molecular Dynamics Study of Montmorillonite Clay: Emergence of Undulatory Fluctuations and Determination of Material Properties. *J. Phys. Chem. C* **2007**, *111*, 8248−8259.
(140) Thyveetil, M. A.; Coveney, P. V.; Suter, J. L.; Greenwell, H. C. Emergence of Undulations and Determination of Material Properties in Large-Scale Molecular Dynamics Simulation of Layered Double Hydroxides. *Chem. Mater.* **2007**, *19*, 5510−5523.
(141) Al-Muhit, B.; Sanchez, F. Nano-Engineering of the Mechanical Properties of Tobermorite 14 Å with Graphene Via Molecular Dynamics Simulations. *Constr. Build. Mater.* **2020**, *233*, 117237.
(142) González, R. I.; Rogan, J.; Bringa, E. M.; Valdivia, J. A. Mechanical Response of Aluminosilicate Nanotubes under Compression. *J. Phys. Chem. C* **2016**, *120*, 14428−14434.
(143) Honorio, T.; Brochard, L.; Vandamme, M.; Lebee, A. Flexibility of Nanolayers and Stacks: Implications in the Nanostructuration of Clays. *Soft Matter* **2018**, *14*, 7354−7367.
(144) Skomorokhov, A. S.; Knizhnik, A. A.; Potapkin, B. V. Molecular Dynamics Study of Ternary Montmorillonite-MT2EtOH-Polyamide-6 Nanocomposite: Structural, Dynamical, and Mechanical Properties of the Interfacial Region. *J. Phys. Chem. B* **2019**, *123*, 2710−2718.
(145) Zhang, J.; Clennell, M. B.; Josh, M.; Pervukhina, M. Frequency and Water Saturation Dependency of Dielectric Properties of Clay Mineral. *Appl. Clay Sci.* **2020**, *198*, 105840.
(146) Swadling, J. B.; Coveney, P. V.; Greenwell, H. C. Clay Minerals Mediate Folding and Regioselective Interactions of RNA: A Large-Scale Atomistic Simulation Study. *J. Am. Chem. Soc.* **2010**, *132*, 13750−13764.
(147) Szczerba, M.; Kalinichev, A. G.; Kowalik, M. Intrinsic Hydrophobicity of Smectite Basal Surfaces Quantitatively Probed by Molecular Dynamics Simulations. *Appl. Clay Sci.* **2020**, *188*, 105497.
(148) Underwood, T. R.; Bourg, I. C. Large-Scale Molecular Dynamics Simulation of the Dehydration of a Suspension of Smectite Clay Nanoparticles. *J. Phys. Chem. C* **2020**, *124*, 3702−3714.
(149) Ho, T. A.; Greathouse, J. A.; Wang, Y. F.; Criscenti, L. J. Atomistic Structure of Mineral Nano-Aggregates from Simulated Compaction and Dewatering. *Sci. Rep.* **2017**, *7*, 15286.
(150) Szczerba, M.; Kalinichev, A. G. Intercalation of Ethylene Glycol in Smectites: Several Molecular Simulation Models Verified by X-Ray Diffraction Data. *Clays Clay Miner.* **2016**, *64*, 488−502.
(151) Szczerba, M.; Kuligiewicz, A.; Derkowski, A.; Gionis, V.; Chryssikos, G. D.; Kalinichev, A. G. Structure and Dynamics of Water-Smectite Interfaces: Hydrogen Bonding and the Origin of the Sharp O-D_w/O-H_w Infrared Band from Molecular Simulations. *Clays Clay Miner.* **2016**, *64*, 452−471.
(152) Pouvreau, M.; Greathouse, J. A.; Cygan, R. T.; Kalinichev, A. G. Structure of Hydrated Gibbsite and Brucite Edge Surfaces: DFT Results and Further Development of the ClayFF Classical Force Field with Metal-O-H Angle Bending Terms. *J. Phys. Chem. C* **2017**, *121*, 14757−14771.
(153) Pouvreau, M.; Greathouse, J. A.; Cygan, R. T.; Kalinichev, A. G. Structure of Hydrated Kaolinite Edge Structures: DFT Results and Further Development of the ClayFF Classical Force Field with Metal-O-H Angle Bending Terms. *J. Phys. Chem. C* **2019**, *123*, 11628−11638.
(154) Guimarães, V.; Rodríguez-Castellón, E.; Algarra, M.; Rocha, F.; Bobos, I. Influence of pH, Layer Charge Location and Crystal Thickness Distribution on U(VI) Sorption onto Heterogeneous Dioctahedral Smectite. *J. Hazard. Mater.* **2016**, *317*, 246−258.
(155) Pecini, E. M.; Avena, M. J. Measuring the Isoelectric Point of the Edges of Clay Mineral Particles: The Case of Montmorillonite. *Langmuir* **2013**, *29*, 14926−14934.
(156) Xu, L.; Tian, J.; Wu, H.; Fang, S.; Lu, Z.; Ma, C.; Sun, W.; Hu, Y. H. Anisotropic Surface Chemistry Properties and Adsorption Behavior of Silicate Mineral Crystals. *Adv. Colloid Interface Sci.* **2018**, *256*, 340−351.
(157) Miller, A. W.; Wang, Y. Radionuclide Interaction with Clays in Dilute and Heavily Compacted Systems: A Critical Review. *Environ. Sci. Technol.* **2012**, *46*, 1981−1994.
(158) Montavon, G.; Lerouge, C.; David, K.; Ribet, S.; Hassan-Loni, Y.; Leferrec, M.; Bailly, C.; Robinet, J.-C.; Grambow, B. Nickel Retention on Callovo-Oxfordian Clay: Applicability of Existing Adsorption Models for Dilute Systems to Real Compact Rock. *Environ. Sci. Technol.* **2020**, *54*, 12226−12234.
(159) Martins, D. M. S.; Molinari, M.; Goncalves, M. A.; Mirao, J. P.; Parker, S. C. Toward Modeling Clay Mineral Nanoparticles: The Edge Surfaces of Pyrophyllite and Their Interaction with Water. *J. Phys. Chem. C* **2014**, *118*, 27308−27317.
(160) Rotenberg, B.; Marry, V.; Salanne, M.; Jardat, M.; Turq, P. Multiscale Modelling of Transport in Clays from the Molecular to the Sample Scale. *C. R. Geosci.* **2014**, *346*, 298−306.
(161) Sun, L.; Hirvi, J. T.; Schatz, T.; Kasa, S.; Pakkanen, T. A. Estimation of Montmorillonite Swelling Pressure: A Molecular Dynamics Approach. *J. Phys. Chem. C* **2015**, *119*, 19863−19868.
(162) Ho, T. A.; Greathouse, J. A.; Lee, A. S.; Criscenti, L. J. Enhanced Ion Adsorption on Mineral Nanoparticles. *Langmuir* **2018**, *34*, 5926−5934.
(163) Yu, K.; Schmidt, J. R. Elucidating the Crystal Face- and Hydration-Dependent Catalytic Activity of Hydrotalcites in Biodiesel Production. *J. Phys. Chem. C* **2011**, *115*, 1887−1898.
(164) Zeitler, T. R.; Greathouse, J. A.; Cygan, R. T.; Fredrich, J. T.; Jerauld, G. R. Molecular Dynamics Simulation of Resin Adsorption at Kaolinite Edge Sites: Effect of Surface Deprotonation on Interfacial Structure. *J. Phys. Chem. C* **2017**, *121*, 22787−22796.
(165) Zeitler, T. R.; Greathouse, J. A.; Gale, J. D.; Cygan, R. T. Vibrational Analysis of Brucite Surfaces and the Development of an Improved Force Field for Molecular Simulation of Interfaces. *J. Phys. Chem. C* **2014**, *118*, 7946−7953.
(166) Kroutil, O.; Pezzotti, S.; Gaigeot, M. P.; Predota, M. Phase-Sensitive Vibrational SFG Spectra from Simple Classical Force Field Molecular Dynamics Simulations. *J. Phys. Chem. C* **2020**, *124*, 15253−15263.
(167) Shen, Z.; Kerisit, S. N.; Stack, A. G.; Rosso, K. M. Free-Energy Landscape of the Dissolution of Gibbsite at High pH. *J. Phys. Chem. Lett.* **2018**, *9*, 1809−1814.
(168) Teleman, O.; Jönsson, B.; Engström, S. A Molecular Dynamics Simulation of a Water Model with Intramolecular Degrees of Freedom. *Mol. Phys.* **1987**, *60*, 193−203.
(169) Berendsen, H. J. C.; Grigera, J. R.; Straatsma, T. P. The Missing Term in Effective Pair Potentials. *J. Phys. Chem.* **1987**, *91*, 6269−6271.
(170) Jorgensen, W. L.; Chandrasekhar, J.; Madura, J. D.; Impey, R. W.; Klein, M. L. Comparison of Simple Potential Functions for Simulating Liquid Water. *J. Chem. Phys.* **1983**, *79*, 926−935.
(171) Shahriyari, R.; Khosravi, A.; Ahmadzadeh, A. Nanoscale Simulation of Na-Montmorillonite Hydrate under Basin Conditions, Application of CLAYFF Force Field in Parallel GCMC. *Mol. Phys.* **2013**, *111*, 3156−3167.
(172) Li, P.; Roberts, B. P.; Chakravorty, D. K.; Merz, K. M. Rational Design of Particle Mesh Ewald Compatible Lennard-Jones Parameters for + 2 Metal Cations in Explicit Solvent. *J. Chem. Theory Comput.* **2013**, *9*, 2733−2748.
(173) Li, P.; Song, L. F.; Merz, K. M. Systematic Parameterization of Monovalent Ions Employing the Nonbonded Model. *J. Chem. Theory Comput.* **2015**, *11*, 1645−1657.

https://doi.org/10.1021/acs.jpcc.1c04600
J. Phys. Chem. C 2021, 125, 17573−17589

(174) Kraevsky, S. V.; Tournassat, C.; Vayer, M.; Warmont, F.; Grangeon, S.; Wakou, B. F. N.; Kalinichev, A. G. Identification of Montmorillonite Particle Edge Orientations by Atomic-Force Microscopy. *Appl. Clay Sci.* **2020**, *186*, 105442.
(175) Uhlig, M. R.; Benaglia, S.; Thakkar, R.; Comer, J.; Garcia, R. Atomically Resolved Interfacial Water Structures on Crystalline Hydrophilic and Hydrophobic Surfaces. *Nanoscale* **2021**, *13*, 5275−5283.
(176) Umeda, K.; Kobayashi, K.; Minato, T.; Yamada, H. Atomic-Scale 3D Local Hydration Structures Influenced by Water-Restricting Dimensions. *Langmuir* **2018**, *34*, 9114−9121.
(177) Umeda, K.; Zivanovic, L.; Kobayashi, K.; Ritala, J.; Kominami, H.; Spijker, P.; Foster, A. S.; Yamada, H. Atomic-Resolution Three-Dimensional Hydration Structures on a Heterogeneously Charged Surface. *Nat. Commun.* **2017**, *8*, 2111.
(178) Dauber-Osguthorpe, P.; Roberts, V. A.; Osguthorpe, D. J.; Wolff, J.; Genest, M.; Hagler, A. T. Structure and Energetics of Ligand-Binding to Proteins: *Escherichia Coli* Dihydrofolate Reductase Trimethoprim, a Drug-Receptor System. *Proteins: Struct., Funct., Genet.* **1988**, *4*, 31−47.
(179) Suter, J. L.; Groen, D.; Coveney, P. V. Chemically Specific Multiscale Modeling of Clay-Polymer Nanocomposites Reveals Intercalation Dynamics, Tactoid Self-Assembly and Emergent Material Properties. *Adv. Mater.* **2015**, *27*, 966−984.
(180) Jorgensen, W. L.; Maxwell, D. S.; Tirado-Rives, J. Development and Testing of the Opls All-Atom Force Field on Conformational Energetics and Properties of Organic Liquids. *J. Am. Chem. Soc.* **1996**, *118*, 11225−11236.
(181) Yu, Y.; Yang, X. Molecular Simulation of Swelling and Interlayer Structure for Organoclay in Supercritical CO_2. *Phys. Chem. Chem. Phys.* **2011**, *13*, 282−290.
(182) Zhou, Q.; Lu, X.; Liu, X.; Zhang, L.; He, H.; Zhu, J.; Yuan, P. Hydration of Methane Intercalated in Na-Smectites with Distinct Layer Charge: Insights from Molecular Simulations. *J. Colloid Interface Sci.* **2011**, *355*, 237−242.
(183) Rao, Q.; Leng, Y. Methane Aqueous Fluids in Montmorillonite Clay Interlayer under near-Surface Geological Conditions: A Grand Canonical Monte Carlo and Molecular Dynamics Simulation Study. *J. Phys. Chem. B* **2014**, *118*, 10956−10965.
(184) Cygan, R. T.; Guggenheim, S.; Koster van Groos, A. F. Molecular Models for the Intercalation of Methane Hydrate Complexes in Montmorillonite Clay. *J. Phys. Chem. B* **2004**, *108*, 15141−15149.
(185) Yan, K.-F.; Li, X.-S.; Chen, Z.-Y.; Xia, Z.-M.; Xu, C.-G.; Zhang, Z. Molecular Dynamics Simulation of the Crystal Nucleation and Growth Behavior of Methane Hydrate in the Presence of the Surface and Nanopores of Porous Sediment. *Langmuir* **2016**, *32*, 7975−7984.
(186) Cygan, R. T.; Romanov, V. N.; Myshakin, E. M. Molecular Simulation of Carbon Dioxide Capture by Montmorillonite Using an Accurate and Flexible Force Field. *J. Phys. Chem. C* **2012**, *116*, 13079−13091.
(187) Sena, M. M.; Morrow, C. P.; Kirkpatrick, R. J.; Krishnan, M. Supercritical Carbon Dioxide at Smectite Mineral-Water Interfaces: Molecular Dynamics and Adaptive Biasing Force Investigation of CO_2/H_2O Mixtures Nanoconfined in Na-Montmorillonite. *Chem. Mater.* **2015**, *27*, 6946−6959.
(188) Johnston, K.; Herbers, C. R.; van der Vegt, N. F. A. Development of Classical Molecule-Surface Interaction Potentials Based on Density Functional Theory Calculations: Investigation of Force Field Representability. *J. Phys. Chem. C* **2012**, *116*, 19781−19788.
(189) Kerisit, S. Water Structure at Hematite-Water Interfaces. *Geochim. Cosmochim. Acta* **2011**, *75*, 2043−2061.
(190) Ho, T. A.; Criscenti, L. J.; Greathouse, J. A. Revealing Transition States During the Hydration of Clay Minerals. *J. Phys. Chem. Lett.* **2019**, *10*, 3704−3709.
(191) Findley, J. M.; Boulfelfel, S. E.; Fang, H.; Muraro, G.; Ravikovitch, P. I.; Sholl, D. S. A Transferable Force Field for Predicting Adsorption and Diffusion of Hydrocarbons and Small Molecules in Silica Zeolites with Coupled-Cluster Accuracy. *J. Phys. Chem. C* **2021**, *125*, 8418−8429.
(192) Ma, Z.; Gamage, R. P.; Rathnaweera, T.; Kong, L. Review of Application of Molecular Dynamic Simulations in Geological High-Level Radioactive Waste Disposal. *Appl. Clay Sci.* **2019**, *168*, 436−449.
(193) Le Crom, S.; Tournassat, C.; Robinet, J.-C.; Marry, V. Influence of Polarizability on the Prediction of Electrical Double Layer Structure in a Clay Mesopore: A Molecular Dynamics Study. *J. Phys. Chem. C* **2020**, *124*, 6221−6232.
(194) Pitman, M. C.; van Duin, A. C. T. Dynamics of Confined Reactive Water in Smectite Clay-Zeolite Composites. *J. Am. Chem. Soc.* **2012**, *134*, 3042−3053.
(195) Senftle, T. P.; et al. The Reaxff Reactive Force-Field: Development, Applications and Future Directions. *npj Comput. Mater.* **2016**, *2*, 15011.
(196) Daksha, C. M.; Yeon, J.; Chowdhury, S. C.; Gillespie, J. W. Automated Reaxff Parametrization Using Machine Learning. *Comput. Mater. Sci.* **2021**, *187*, 110107.
(197) Guo, F.; Wen, Y.-S.; Feng, S.-Q.; Li, X.-D.; Li, H.-S.; Cui, S.-X.; Zhang, Z.-R.; Hu, H.-Q.; Zhang, G.-Q.; Cheng, X.-L. Intelligent-Reaxff: Evaluating the Reactive Force Field Parameters with Machine Learning. *Comput. Mater. Sci.* **2020**, *172*, 109393.

https://doi.org/10.1021/acs.jpcc.1c04600
J. Phys. Chem. C 2021, 125, 17573−17589

Advances in Clayff Molecular Simulation of Layered and Nanoporous Materials and their Aqueous Interfaces

Randall T. Cygan,[†] Jeffery A. Greathouse,[†] and Andrey G. Kalinichev[‡]

[†]Geochemistry Department, Sandia National Laboratories, Albuquerque, New Mexico, 87185-0754, United States

[‡]Laboratoire SUBATECH (UMR 6457 – Institut Mines-Télécom Atlantique, Université de Nantes, CNRS/IN2P3), 44307, Nantes, France

Supporting Information

Parameters for the Clayff interatomic potentials[1] are provided in Tables S1 and S2. Any differences in parameter values from the original publication are due to reporting of significant digits, roundoff errors, or corrections in transposition of digits. Energy values are presented in kcal/mol, distances in Ångstroms, and angles in degrees. Note that values for bond-angle bend force constants incorporate radian units, and conversion between degrees and radians is accommodated in the force constant value. Table S1 includes nonbonded interaction parameters using ε and σ convention for the Lennard-Jones (L-J) potential. The original Clayff publication reported values for L-J potentials using the alternative D_o and R_o convention where $D_o = \varepsilon$ and $R_o = 2^{1/6}\sigma$.

Total potential energy of a molecular system is represented in Clayff as the summation of contributing energy components as described by Equation S1:

$$E_{Total} = E_{Coul} + E_{VDW} + E_{Bond} + \cdots \quad \text{(S1)}$$

The total energy includes contributions from Coulombic, van der Waals, and bonded energy terms. Additional energy terms can be added to Equation S1 to incorporate pressure, stress,

electric fields, and other environmental variables. The potential energy for Coulombic interactions is given as:

$$E_{Coul} = \frac{e^2}{4\pi\epsilon_\circ}\sum_{i\neq j}\frac{q_i q_j}{r_{ij}} \tag{S2}$$

where q_i and q_j are the partial charges for atoms i and j separated by distance r_{ij}. The E_{VDW} term is often incorporated in Equation S1 as a L-J potential to represent short range interactions between atom pairs. It is presented in Equation S3 using ε and σ notation:

$$E_{VDW} = \sum_{i\neq j} 4\varepsilon_{ij}\left[\left(\frac{\sigma_{ij}}{r_{ij}}\right)^{12} - \left(\frac{\sigma_{ij}}{r_{ij}}\right)^{6}\right] \tag{S3}$$

where ε_{ij} is the depth of the potential well and σ_{ij} is the zero-crossing distance for the energy. Combining rules for the L-J parameters are used to mix nonequivalent (off-diagonal) atomic interactions thereby requiring reporting of only the single (diagonal) parameters (Table S1):

$$\sigma_{ij} = \frac{\sigma_i+\sigma_j}{2} \qquad \varepsilon_{ij} = \left(\varepsilon_i\varepsilon_j\right)^{1/2} \tag{S4}$$

Clayff implements a conventional geometric mean for the energy term ε_{ij} and an arithmetic mean for the zero-crossing distance σ_{ij}. A Simple Point Charge (SPC) model[2] is used for the L-J parameters of water molecules in Clayff. Improvements in modeling water polarization using the effective pair potential of the SPC/E water model[3] can be also used with Clayff potentials, however the SPC/E partial charges are not fully consistent with the charges associated with the framework oxygen atoms (see Table S1).

Table S2 presents the bonded parameters for Clayff potentials. A harmonic potential is used to describe the potential energy of -O–H bonds associated with water and hydroxyl groups:

$$E_{harmonic\ stretch} = k_1(r - r_o)^2 \tag{S5}$$

where r_o is the equilibrium bond distance. Similarly, a harmonic function is used to describe the potential energy for the bond-angle bend for water molecules and for selected metal hydroxyl groups (edges and truncated surfaces):

$$E_{harmonic\ bend} = k_2(\theta - \theta_o)^2 \quad \text{(S6)}$$

where θ_o represents the equilibrium bond angle for a three-body interaction. Full flexibility of water molecules is therefore incorporated in Clayff by use of harmonic bond stretch and bond-angle bending terms.[4] A Morse potential has been successfully used in Clayff simulations of clay minerals involving TOT layers with dioctahedral and trioctahedral structures:

$$E_{Morse\ stretch} = D_o\left[1 - e^{-\alpha(r-r_o)}\right]^2 \quad \text{(S7)}$$

where D_o is the dissociation energy, r_o is the equilibrium bond distance, and α is an additional fitting parameter representing the width of the potential energy well. Use of a Morse potential for modeling hydroxyl groups has led to improved simulations of vibrational spectra for TOT clay minerals.[5]

Recognizing the challenge of modeling edge sites of layered phases and other complex materials, Clayff has been recently updated to accurately predict the librational motions of hydroxyl groups associated with edges and other truncated surfaces.[6-8] Harmonic bond-angle bend terms (Equation S6) were parameterized from results of DFT-MD simulations and were optimized to accurately predict structure and power spectra. Force constants and equilibrium bond angles are presented in Table S2 for selected metal atom types associated with protonated oxygen species. Note, these bonded M-O-H parameters replace the three-body parameters published in the original Clayff potential set, which were cast in a different functional form and difficult to implement in practice. They can be implemented as special nonbonded three-body terms (*e.g.*, LAMMPS "pair style nb3b/harmonic"; Materials Studio Forcite "NON-

BONDED_3-BODY"). These M-O-H parameters can also be implemented as angle terms without associated bond terms, thereby bypassing the standard 1-3 or 1-4 bond exclusion rules. However, in this case, the angle terms continue to be evaluated even when the hydroxyl group moves away from the metal (M) during the simulation.

Clayff potentials are typically assigned as atom types in molecule models involving simulation cells with periodic boundary conditions. Some graphical-based software packages, such as Materials Studio, require molecular models be created without bonds for the metal-oxygen framework so that the nonbonded Clayff potentials are properly implemented. Water molecules and hydroxyl groups would require graphical bonds, and have corresponding bonded potentials (bond stretch and bond-angle bend) for evaluating their bond energy contributions. There are several pre- and post-processing software tools available to the user for preparing molecular models for Clayff-based simulations and for analyzing molecular structures from atomic trajectories obtained from MD simulations.[9-11] Many of these tools are developed by academic institutions and are customized for specific applications. An open-source MATLAB library has been recently developed by Holmboe[12] to create models of layered minerals and other phases, to assign Clayff attributes, to protonate and solvate models, and to analyze bonding and atomic structure for models from multiple simulations.

Table S1. Nonbond Parameters for the Clayff Force Field

species	symbol	charge (e)	ε (kcal/mol)	σ (Å)
SPC water hydrogen	h*	0.4100		
SPC water oxygen	o*	-0.8200	0.1554	3.1655
SPC/E water hydrogen	h*	0.4238		
SPC/E water oxygen	o*	-0.8476	0.1554	3.1655
hydroxyl hydrogen	ho	0.4250		
hydroxyl oxygen	oh	-0.9500	0.1554	3.1655
bridging oxygen	ob	-1.0500	0.1554	3.1655
bridging oxygen with octahedral substitution	obos	-1.1808	0.1554	3.1655
bridging oxygen with tetrahedral substitution	obts	-1.1688	0.1554	3.1655
bridging oxygen with double substitution	obss	-1.2996	0.1554	3.1655
hydroxyl oxygen with substitution	ohs	-1.0808	0.1554	3.1655
tetrahedral silicon	st	2.1000	1.8405×10^{-6}	3.3020
octahedral aluminum	ao	1.5750	1.3298×10^{-6}	4.2712
tetrahedral aluminum	at	1.5750	1.8405×10^{-6}	3.3020
octahedral magnesium	mgo	1.3600	9.0298×10^{-7}	5.2643
hydroxide magnesium	mgh	1.0500	9.0298×10^{-7}	5.2643
octahedral calcium	cao	1.3600	5.0298×10^{-6}	5.5667
hydroxide calcium	cah	1.0500	5.0298×10^{-6}	5.5667
octahedral iron	feo	1.5750	9.0298×10^{-7}	4.9062
octahedral lithium	lio	0.5250	9.0298×10^{-7}	4.2101
aqueous sodium ion	Na	1.0	0.1301	2.3500
aqueous potassium ion	K	1.0	0.1000	3.3340
aqueous cesium ion	Cs	1.0	0.1000	3.8310
aqueous calcium ion	Ca	2.0	0.1000	2.8720
aqueous barium ion	Ba	2.0	0.0470	3.8166
aqueous chloride ion	Cl	-1.0	0.1001	4.4000

Table S2. Bond Parameters for the Clayff Force Field

harmonic bond stretch			k_1	r_o
	species *i*	species *j*	(kcal/mol Å^2)	(Å)
SPC	o*	h*	554.1349	1.0000
SPC/E	o*	h*	554.1349	1.0000
	oh	ho	554.1349	1.0000
	ohs	ho	554.1349	1.0000

harmonic bond-angle bend				k_2	θ_o
	species *i*	species *j*	species *k*	(kcal/mol rad^2)	(deg)
SPC	h*	o*	h*	45.7696	109.47
SPC/E	h*	o*	h*	45.7696	109.47

Morse bond stretch			D_o	α	r_o
	species *i*	species *j*	(kcal/mol)	(Å^{-1})	(Å)
dioctahedral	oh	ho	132.2491	2.1815	0.9450
trioctahedral	oh	ho	132.2491	2.1350	0.9572

M-O-H harmonic bond-angle bend				k_2	θ_o
	species *i*	species *j*	species *k*	(kcal/mol rad^2)	(deg)
	st	oh	ho	15.0	100.0
bulk	ao	oh	ho	15.0	116.0
surface	ao	oh	ho	15.0	110.0
bulk	mgo	oh	ho	6.0	120.0
surface	mgo	oh	ho	6.0	110.0

SAMPLE CLAYFF INPUT FILES

Several sample program input files incorporating Clayff parameters are provided below to assist the user in implementing Clayff in commonly-used classical mechanics and molecular simulation software packages. The software programs include LAMMPS, GROMACS, and Materials Studio modules Forcite and Discover. Please note the following:

- Other ion-water parameters[13-16] in the LJ 6-12 format could be used in place of (or in addition to) the VDW parameters provided in the original Clayff set. Off-diagonal parameters for ion-mineral interactions can then be derived using the appropriate mixing rules.
- Some software packages have options for automated assignment of atom types (partial charges, L-J parameters). These parameter assignments should always be checked since the algorithms may not be appropriate for all model systems.

- There may be subtle differences in parameter values between the sample input files for these codes and those provided in Tables S1 and S2. Often such input files are recreated as restart files during program execution and often include extraneous significant digits for the Clayff parameters.
- Nothing is guaranteed in these examples, and the software user is reminded to consult the original publications (including this review article) and the software manuals to ensure that parameter choices and program options are appropriately implemented for the technical problem at hand.

Clayff for LAMMPS

```
LAMMPS

Pair Coeffs # lj/cut/coul/long

   1   0.0000018402   3.3019566252 # st tetrahedral Si         2.1
   2   0.0000013297   4.2713219316 # ao octahedral Al          1.575
   3   0.0000018402   3.3019566252 # at tetrahedral Al         1.575
   4   0.0000009030   5.2643258688 # mgo octahedral Mg         1.36
   5   0.0000009030   5.2643258688 # mgh hydroxide Mg          1.05
   6   0.0000050301   5.5666638636 # cao octahedral Ca         1.36
   7   0.0000050219   5.5624343529 # cah hydroxide Ca          1.05
   8   0.0000009030   4.9057651456 # feo octahedral Fe         1.575
   9   0.0000009030   4.2105948665 # lio octahedral Li         0.525
  10   0.1554164124   3.1655200879 # ob bridging oxygen      -1.05
  11   0.1554164124   3.1655200879 # obss oxygen double sub. -1.2996
  12   0.1554164124   3.1655200879 # obts oxygen tet. sub.   -1.1688
  13   0.1554164124   3.1655200879 # obos oxygen oct. sub.   -1.1808
  14   0.1554164124   3.1655200879 # ohs hydroxyl O sub.     -1.0808
  15   0.1554164124   3.1655200879 # oh hydroxyl O           -0.95
  16   0.1554164124   3.1655200879 # o* spc water O          -0.82
  17   0.0000000000   0.0000000000 # ho hydroxyl H            0.425
  18   0.0000000000   0.0000000000 # h* spc water H           0.41
  19   0.1300999871   2.3500126639 # Na sodium ion            1.0
  20   0.1000015417   3.3340059879 # K potassium ion          1.0
  21   0.1000007161   3.8310403819 # Cs cesium ion            1.0
  22   0.0999999980   2.8719902024 # Ca calcium ion           2.0
  23   0.0470957194   3.8166120025 # Ba barium ion            2.0
  27   0.1000998933   4.3999709805 # Cl chloride ion         -1.0

Bond Coeffs # harmonic

   1     553.935    1.0000 # o*-h*
   2     553.935    1.0000 # oh-ho
   3     553.935    1.0000 # ohs-ho

Bond Coeffs # morse

   1     132.2491   2.1815 0.9450   # oh-ho or ohs for dioctahedral clays
   2     132.2491   2.1350 0.9572   # oh-ho or ohs for trioctahedral clays

Angle Coeffs # harmonic
```

```
  1     45.753     109.47 # h*-o*-h*
  2     15.000     110.00 # ao-oh ho or ao-ohs-ho for surface hydroxyls
  3     15.000     116.00 # ao-oh ho or ao-ohs-ho for bulk hydroxyls
  4      6.000     110.00 # mgo-oh ho or ao-ohs-ho for surface hydroxyls
  5      6.000     120.00 # mgo-oh ho or ao-ohs-ho for bulk hydroxyls
  6     15.000     100.00 # st-oh ho or st-ohs-ho for bulk or surface hydroxyls
```

Clayff for Materials Studio Forcite

```
VERSION 3.1.02
 CERIUS2     1
END
#
HEADER
END
#
PREFERENCES
 BONDS                                T
 ANGLES                               T
 COULOMB                              T
 INVERSIONS                           F
 TORSIONS                             T
 UREY_BRADLEY                         F
 STRETCH_STRETCH                      F
 SEPARATED_STRETCH_STRETCH            F
 STRETCH_BEND_STRETCH                 F
 BEND_BEND                            F
 TORSION_STRETCH                      F
 TORSION_BEND_BEND                    F
 BEND_TORSION_BEND                    F
 STRETCH_TORSION_STRETCH              F
 HYDROGEN_BONDS                       F
 DIAGONAL_VAN_DER_WAALS               T
 OFF_DIAGONAL_VAN_DER_WAALS           T
 IGNORE_UNDEFINED_TERMS               T
 NON-BONDED_3-BODY                    F
 SHRINK_CH_BONDS                      F
 SHRINK_CH_H_ATOM                     H__C
 SHRINK_CH_FACTOR                        0.91500
 SINGLE_TORSION                       F
 SCALE_TORSIONS_ABOUT_COMMON_BOND     F
 SCALE_BY_N_DEFINED_TORSIONS          T
 EXOCYCLIC_TORSIONS_SCALE_FACTOR         0.40000
 SINGLE_INVERSION                     F
 H-BOND_METHOD                        SPLINE
 H-BOND_LIST                          T
 H-BOND_DIRECT_RCUT                      4.00000
 H-BOND_SPLINE_DISTANCE_ON               4.00000
 H-BOND_SPLINE_DISTANCE_OFF              4.50000
 H-BOND_SPLINE_ANGLE_ON                 65.00000
 H-BOND_SPLINE_ANGLE_OFF                75.00000
 H-BOND_LIST_DISTANCE_OFF                6.50000
 H-BOND_LIST_ANGLE_OFF                  90.00000
 NB_NEIGHBOUR_SEARCH_METHOD           LIST
 NON_BOND_BUFFER_DISTANCE                2.00000
 H-BOND_BUFFER_DISTANCE                  2.00000
 COU_DIELETRIC_CONSTANT                    1.00000000000000000
 COU_INTER_CUT_OFF                       8.00000
 COU_SPLINE_OFF                          8.50000
 COU_SPLINE_ON                           8.00000
 EWALD_SUM_COU_ACCURACY                  0.00100
 EWALD_SUM_COU_ETA                       3.20600
 EWALD_SUM_COU_KCUT                      0.40900
 EWALD_SUM_COU_RCUT                     10.85000
 EWALD_SUM_COU_OPTIMIZE               SMART
 COU_EXCLUDE_1-2                      T
 COU_EXCLUDE_1-3                      T
 COU_EXCLUDE_1-4                      F
 COU_1-4_SCALE_FACTOR                    1.00000
```

```
 COU_METHOD                          EWALD
 COU_DIRECT_CUT-OFF                     8.00000
 VDW_COMBINATION_RULE                ARITHMETIC
 VDW_INTER_CUT_OFF                      8.00000
 VDW_EXCLUDE_1-2                     T
 VDW_EXCLUDE_1-3                     T
 VDW_EXCLUDE_1-4                     F
 VDW_1-4_SCALE_FACTOR                   1.00000
 VDW_METHOD                          SPLINE
 VDW_SPLINE_ON                          8.00000
 VDW_SPLINE_OFF                         8.50000
 EWALD_SUM_VDW_OPTIMIZE              SMART
 EWALD_SUM_VDW_ACCURACY                 0.00100
 EWALD_SUM_VDW_ETA                      1.98000
 EWALD_SUM_VDW_KCUT                     0.56000
 EWALD_SUM_VDW_RCUT                     5.50000
 EWALD_SUM_VDW_REP_CUT                  6.40000
 FAST_EWALD_SUM_RATIO                  10.00000
 SLOW_EWALD_SUM_RATIO                   5.00000
 MINIMUM_IMAGE                       F
 ASSIGN_MASS                         F
 ASSIGN_CHARGE                       F
 ASSIGN_HYBRIDIZATION                F
 ASSIGN_VALBOND_CENTER               F
 ATOM_TYPE                           F
 ATOM_TYPE_ALL                       T
 CALCULATE_BOND_ORDER                F
END
#
ATOMTYPES
 h*         H       1.00790  0.4100   1   0   0  ! spc water H
 ho         H       1.00794  0.4250   1   0   0  ! hydroxyl H
 o*         O      15.99940 -0.8200   3   0   0  ! spc water O
 oh         O      15.99940 -0.9500   3   0   0  ! hydroxyl O
 ob         O      15.99940 -1.0500   3   0   0  ! bridging oxygen
 st         Si     28.08550  2.1000   3   0   0  ! tetrahedral Si
 ao         Al     26.98154  1.5750   6   0   0  ! octahedral Al
 at         Al     26.98154  1.5750   3   0   0  ! tetrahedral Al
 mgo        Mg     24.30500  1.3600   3   0   0  ! octahedral Mg
 cao        Ca     40.08000  1.3600   6   0   0  ! octahedral Ca
 feo        Fe     55.84700  1.5750   6   0   0  ! octahedral Fe
 lio        Li      6.94000  0.5250   0   0   0  ! octahedral Li
 obss       O      15.99940 -1.2996   2   0   0  ! oxygen double sub.
 obts       O      15.99940 -1.1688   2   0   0  ! oxygen tet. sub.
 obos       O      15.99940 -1.1808   2   0   0  ! oxygen oct. sub.
 ohs        O      15.99940 -1.0808   2   0   0  ! hydroxyl O sub.
 cah        Ca     40.08000  1.0500   6   0   0  ! hydroxide Ca
 mgh        Mg     24.30500  1.0500   3   0   0  ! hydroxide Mg
 Na         Na     22.98977  1.0000   7   0   0  ! sodium ion
 K          K      39.09830  1.0000   0   0   0  ! potassium ion
 Cs         Cs    132.90546  1.0000   0   0   0  ! cesium ion
 Ca         Ca     40.08000  2.0000   6   0   0  ! calcium ion
 Ba         Ba    137.33000  2.0000   7   0   0  ! barium ion
 Cl         Cl     35.45270 -1.0000   0   0   0  ! chloride ion
END
#
DIAGONAL_VDW
 h*          IGNORE        4.577499866485596
 ho          IGNORE        4.577499866485596
 o*          LJ_6_12       3.553200006484985       0.1553999930620193
 oh          LJ_6_12       3.553200006484985       0.1553999930620193
 ob          LJ_6_12       3.553200006484985       0.1553999930620193
 st          LJ_6_12       3.706350088119507       0.1840499976424326E-05
 ao          LJ_6_12       4.794320106506348       0.1329800056737440E-05
 at          LJ_6_12       3.706350088119507       0.1840499976424326E-05
 mgo         LJ_6_12       5.909016132354736       0.9029800480675476E-06
 cao         LJ_6_12       6.248403072357178       0.5029799922340317E-05
 feo         LJ_6_12       5.507011890411377       0.9029800480675476E-06
 lio         LJ_6_12       4.725677013397217       0.9029799912241288E-06
 obss        LJ_6_12       3.553200006484985       0.1553999930620193
 obts        LJ_6_12       3.553200006484985       0.1553999930620193
 obos        LJ_6_12       3.553200006484985       0.1553999930620193
 ohs         LJ_6_12       3.553200006484985       0.1553999930620193
```

```
 cah          LJ_6_12        6.242803096771240       0.5029799922340317E-05
 mgh          LJ_6_12        5.909016132354736       0.9029799912241288E-06
 Na           LJ_6_12        2.637800011444092       0.1300999969244003
 K            LJ_6_12        3.742300000000000       0.1000000000000000
 Cs           LJ_6_12        4.300200000000000       0.1000000000000000
 Ca           LJ_6_12        3.223700000000000       0.1000000000000000
 Ba           LJ_6_12        4.284000000000000       0.0470960000000000
 Cl           LJ_6_12        4.938800000000000       0.1001000001692772
END
#
ATOM_TYPING_RULES
 h*               H              0              0              1              1
                  O              1              0              1              1
                  H              0              0              1              1
                  **             0              0              0             -1
 o*               O              0              0              2              1
                  H              0              0              0              1
                  H              0              0              0              1
 ob               O              0              0              1              1
                  H              0              0              0             -1
 st               Si             3              0              1              1
                  O              0              0              0              1
 ao               Al             6              0              1              1
                  O              0              0              0              1
 at               Al             3              0              1              1
                  O              0              0              0              1
 Na               Na             0              0              0              1
 K                K              0              0              0              1
 Cs               Cs             0              0              0              1
 Ca               Ca             0              0              0              1
 Ba               Ba             0              0              0              1
 Cl               Cl             0              0              0              1
 Mg               Mg             0              0              0              1
 mgo              Mg             0              0              0              1
 cao              Ca             0              0              0              1
 feo              Fe             6              0              0              1
 lio              Li             6              0              0              1
 oh               O              0              0              3              1
                  H              0              0              0              1
                  **             6              0              0              1
                  **             6              0              0              1
 ho               H              0              0              1              1
                  O              0              0              1              1
                  **             6              0              0              1
 ohs              O              0              0              2              1
                  H              0              0              0              1
                  Mg             6              0              0              1
 obts             O              0              0              2              1
                  Al             3              0              0              1
                  **             0              0              0              1
 obos             O              0              0              2              1
                  Al             6              0              0              1
                  Mg             6              0              0              1
 obss             O              0              0              3              1
                  Al             3              0              0              1
                  Mg             6              0              0              1
                  **             6              0              0              1
 cah              Ca             6              0              1              1
                  O              0              0              1              1
                  Ca             6              0              0              1
 mgh              Mg             6              0              1              1
                  O              0              0              1              1
                  Mg             6              0              0              1
END
#
#
OFF_DIAGONAL_VDW
END
#
BOND_STRETCH
 o*       h*          HARMONIC    1108.2697    1.0000
 oh       ho          HARMONIC    1108.2697    1.0000
 ohs      ho          HARMONIC    1108.2697    1.0000
```

```
 oh       ho          MORSE       132.2491   2.1815 0.9450 0.00000 ! oh-ho or ohs for
dioctahedral clays
 ohs      ho          MORSE       132.2491   2.1350 0.9572 0.00000 ! oh-ho or ohs for
trioctahedral clays
END
#
ANGLE_BEND
 h*       o*       h*          THETA_HARM    91.5392  109.4700
END
#
#
NON-BONDED_3-BODY
 ao       oh       ho          HARMONIC      30.0000    110.00  ! surface hydroxyls
 ao       ohs      ho          HARMONIC      30.0000    110.00  ! surface hydroxyls
 ao       oh       ho          HARMONIC      30.0000    116.00  ! bulk hydroxyls
 ao       ohs      ho          HARMONIC      30.0000    116.00  ! bulk hydroxyls
 mgo      oh       ho          HARMONIC      12.0000    110.00  ! surface hydroxyls
 mgo      ohs      ho          HARMONIC      12.0000    110.00  ! surface hydroxyls
 mgo      oh       ho          HARMONIC      12.0000    120.00  ! bulk hydroxyls
 mgo      ohs      ho          HARMONIC      12.0000    120.00  ! bulk hydroxyls
 st       oh       ho          HARMONIC      30.0000    100.00  ! bulk or surface hydroxyls
 st       ohs      ho          HARMONIC      30.0000    100.00  ! bulk or surface hydroxyls
END
#
COULOMBIC
 X        X           CONST-EPS
END
```

Clayff for Materials Studio Discover

```
! Discover .frc

#atom_types

!Ver  Ref  Type    Mass      Element  Connections   Description and charge
!---- ---  ----  ----------  -------  -----------------------------------------
 1.0  --    st     28.08550    Si          4        tetrahedral silicon  2.1
 1.0  --    ao     26.98154    Al          6        octahedral aluminum  1.575
 1.0  --    at     26.98154    Al          4        tetrahedral aluminum 1.575
 1.0  --   mgo     24.30500    Mg          6        octahedral magnesium 1.36
 1.0  --   mgh     24.30500    Mg          6        hydroxide magnesium  1.05
 1.0  --   cao     40.08000    Ca          6        octahedral calcium   1.36
 1.0  --   cah     40.08000    Ca          6        hydroxide calcium    1.05
 1.0  --   feo     55.84700    Fe          6        octahedral iron      1.575
 1.0  --   lio     6.941000    Li          6        octahedral lithium   0.525
 1.0  --    ob    15.99940      O          2        bridging oxygen     -1.05
 1.0  --  obss     15.99940      O          3        oxygen double sub.  -1.2996
 1.0  --  obts     15.99940      O          2        oxygen tet. sub.    -1.1688
 1.0  --  obos     15.99940      O          2        oxygen oct. sub.    -1.1808
 1.0  --   ohs     15.99940      O          2        hydroxyl O sub.     -1.0808
 1.0  --    oh     15.99940      O          2        hydroxyl O          -0.95
 1.0  --    o*     15.99940      O          2        spc water O         -0.82
 1.0  --    ho     1.007970      H          1        hydroxyl H           0.425
 1.0  --    h*     1.007970      H          1        spc water H          0.41
 1.0  --    Na     22.99000     Na          0        sodium ion           1.0
 1.0  --     K     39.10         K          0        potassium ion        1.0
 1.0  --    Cs     132.9100     Cs          0        cesium ion           1.0
 1.0  --    Ca     40.07980     Ca          0        calcium ion          2.0
 1.0  --    Ba     137.3300     Ba          0        barium ion           2.0
 1.0  --    Cl     35.45300     Cl          0        chloride ion        -1.0


#quadratic_bond

> E = K2 * (R - R0)^2

!Ver  Ref     I     J          R0         K2
!---- ---    ----  ----     -------    --------
 1.0  --      o*   h*        1.0000    553.9350
 1.0  --      oh   ho        1.0000    553.9350
```

```
 1.0  --     ohs   ho        1.0000    553.9350


#morse_bond

> E = D * (1 - exp(-ALPHA*(R - R0)))^2

!Ver  Ref     I     J          R0         D           ALPHA
!---- ---    ----  ----     -------    --------      -------
 1.0  --     oh    ho        0.9450    132.2491      2.1815
 1.0  --     ohs   ho        0.9572    132.2491      2.1350


#quadratic_angle

> E = K2 * (Theta - Theta0)^2

!Ver  Ref     I     J     K       Theta0         K2
!---- ---    ----  ----  ----    --------     -------
 1.0   1     h*    o*    h*      109.4700     45.7530
 1.0   1     ao    oh    ho      110.0        15.0      ! surface hydroxyls
 1.0   1     ao    ohs   ho      110.0        15.0      ! surface hydroxyls
 1.0   1     ao    oh    ho      116.0        15.0      ! bulk hydroxyls
 1.0   1     ao    oh    ho      116.0        15.0      ! bulk hydroxyls
 1.0   1    mgo    oh    ho      110.0        12.0      ! surface hydroxyls
 1.0   1    mgo    ohs   ho      110.0        12.0      ! surface hydroxyls
 1.0   1    mgo    oh    ho      120.0        12.0      ! bulk hydroxyls
 1.0   1    mgo    oh    ho      120.0        12.0      ! bulk hydroxyls
 1.0   1     st    oh    ho      100.0        15.0      ! surface or bulk hydroxyls
 1.0   1     st    ohs   ho      100.0        15.0      ! surface or bulk hydroxyls


#nonbond(12-6)

@type A-B
@combination geometric

> E = Aij/r^12 - Bij/r^6
> where  Aij = sqrt( Ai * Aj )
>        Bij = sqrt( Bi * Bj )

!Ver  Ref     I           A             B
!---- ---    ----    -----------   -----------
 1.0   1    st           12.3645       0.00954
 1.0   1    ao          196.1446       0.03230
 1.0   1    at           12.3645       0.00954
 1.0   1   mgo         1636.3265       0.07688
 1.0   1   mgh         1636.3265       0.07688
 1.0   1   cao         17814.73        0.5987
 1.0   1   cah         17624.076       0.595
 1.0   1   feo           702.54        0.0504
 1.0   1   lio           112.01        0.0201
 1.0   1    ob      629358.0000     625.50000
 1.0   1  obss      629358.0000     625.50000
 1.0   1  obts      629358.0000     625.50000
 1.0   1  obos      629358.0000     625.50000
 1.0   1   ohs      629358.0000     625.50000
 1.0   1    oh      629358.0000     625.50000
 1.0   1    o*      629358.0000     625.50000
 1.0   1    ho        0.00000001       0.00000
 1.0   1    h*        0.00000001       0.00000
 1.0   1    Na       14763.1719      87.65132
 1.0   1    K        754506.86       549.37
 1.0   1    Cs       3998193.96     1264.63
 1.0   1    Ca      125966.6068     224.46969
 1.0   1    Ba      1799606.56      582.25
 1.0   1    Cl      21081006.97     2905.31
```

Clayff for GROMACS

forcefield.itp

```
#define _ClayFF
;[ defaults ]
; nbfunc       comb-rule      gen-pairs      fudgeLJ fudgeQQ
;1                    2                     yes                    1.0            1.0
#include "./ffnonbonded.itp"
#include "./ions.itp"
```

ffclayff.atp

```
   hw   1.008          ; water hydrogen
   ho   1.008          ; hydroxyl hydrogen
   ow   16.00          ; water hydrogen
   oh   16.00          ; hydroxyl oxygen
   ob   16.00          ; bridging oxygen
   obos 16.00          ; bridging oxygen with octahedral substitution
   obts 16.00          ; bridging oxygen with tetrahedral substitution
   obss 16.00          ; bridging oxygen with double substitution
   ohs  16.00          ; hydroxyl oxygen with substitution
   st   28.09          ; tetrahedral silicon
   ao   26.98          ; octahedral aluminum
   at   26.98          ; tetrahedral aluminum
   mgo  24.31          ; octahedral magnesium
   mgh  24.31          ; hydroxide magnesium
   cao  40.08          ; octahedral calcium
   cah  40.08          ; hydroxide calcium
   feo  55.85          ; octahedral iron
   lio  6.941          ; octahedral lithium
   Na   22.99          ; aqueous sodium ion
   K    39.10          ; aqueous potassium ion
   Cs   132.9          ; aqueous cesium ion
   Ca   40.08          ; aqueous calcium ion
   Ba   137.3          ; aqueous barium ion
   Cl   35.45          ; aqueous chloride ion
```

ffnonbonded.itp

```
[ atomtypes ]
; atom descriptions and masses are assigned in ffclayff.atp
; name  at.numb.mass   charge  ptype          sigma                 epsilon
   Hw   1       1.008   0.4100  A             0.0                   0.0
   ho   1       1.008   0.4250  A             0.0                   0.0
   ow   8       16.000  -0.8200 A             3.1655E-01            6.502E-01
   oh   8       16.000  -0.9500 A             3.1655E-01            6.502E-01
   ob   8       16.000  -1.0500 A             3.1655E-01            6.502E-01
   obos 8       16.000  -1.1808 A             3.1655E-01            6.502E-01
   obts 8       16.000  -1.1688 A             3.1655E-01            6.502E-01
   obss 8       16.000  -1.2996 A             3.1655E-01            6.502E-01
   ohs  8       16.000  -1.0808 A             3.1655E-01            6.502E-01
   st   16      28.090  2.1000  A             3.3020E-01            7.701E-06
   ao   13      26.980  1.5750  A             4.2712E-01            5.564E-06
   at   13      26.980  1.5750  A             3.3020E-01            7.701E-06
   mgo  12      24.310  1.3600  A             5.2643E-01            3.778E-06
   mgh  12      24.310  1.0500  A             5.2643E-01            3.778E-06
   cao  20      40.080  1.3600  A             5.5667E-01            2.104E-05
   cah  20      40.080  1.0500  A             5.5617E-01            2.104E-05
   feo  26      55.850  1.5750  A             4.9062E-01            3.778E-06
   lio  3       6.941   0.5250  A             4.2101E-01            3.778E-06
   Na   11      22.990  1.0000  A             2.3500E-01            5.443E-01
   k    19      39.100  1.0000  A             3.3340E-01            4.184E-01
   Cs   55      132.900 1.0000  A             3.8310E-01            4.184E-01
   Ca   20      40.080  2.0000  A             2.8720E-01            4.184E-01
   Ba   56      137.300 2.0000  A             3.8166E-01            1.966E-01
   Cl   17      34.450  -1.0000 A             4.4000E-01            4.188E-01
```

ffbonded.itp

```
; Bond type code
 ; when converting from ClayFF to Gromacs use 1cal - 4.186 J
 ; also need to multiply k by 2
 ;
 #define oh        0.1  463532.8
 ; hydroxil bond
 ;
#define ohs        0.1  463532.8
 ; hydroxil bond with substitution
 ;
#define ohw        0.1  463532.8
 ; water bond
 ;
 ;
 ;for konversion use 1 kcal/mol A^2 = 418.6 kJ/mol nm^2
 ;also multiply by 2
 ;
 ; Bond-angle type code
 ;
 #define hoh         109.47  383.0
 ; water angle
 ;
 #define moh         109.47  251.2
 ; metal-oh
 ;
```

spc.itp

```
[ moleculetype ]
; molname      nrexcl
SOL            2

[ atoms ]
;   nr   type  resnr residue  atom   cgnr     charge       mass
     1     OW      1    SOL     OW      1      -0.82
     2     HW      1    SOL    HW1      1       0.41
     3     HW      1    SOL    HW2      1       0.41

#ifndef FLEXIBLE
[ settles ]
; OW    funct   doh     dhh
1       1       0.1     0.16330

[ exclusions ]
1       2       3
2       1       3
3       1       2
#else
[ bonds ]
; i     j       funct   length  force.c.
1       2       1       0.1     345000  0.1     345000
1       3       1       0.1     345000  0.1     345000

[ angles ]
; i     j       k       funct   angle   force.c.
2       1       3       1       109.47  383     109.47  383
#endif
```

ions.itp

```
[ moleculetype ]
; molName       nrexcl
k               1

[ atoms ]
; id    at type res nr  residu Name     at Name  cg nr   charge
1       k       1       k               k        1       1

[ moleculetype ]
```

```
; molName   nrexcl
Na          1

[ atoms ]
; id    at type res nr  residu Name at Name  cg nr  charge
1       Na      1       Na          Na       1      1

[ moleculetype ]
; molName   nrexcl
Ca          1

[ atoms ]
; id    at type res nr  residu Name at Name  cg nr  charge
1       Ca      1       Ca          Ca       1      2

[ moleculetype ]
; molName   nrexcl
Cl          1

[ atoms ]
; id    at type res nr  residu Name at Name  cg nr  charge
1       Cl      1       Cl          Cl       1      -1

[ moleculetype ]
; molName   nrexcl
Cs          1

[ atoms ]
; id    at type res nr  residu Name at Name  cg nr  charge
1       Cs      1       Cs          Cs       1      1
```

ffMontUC.itp

```
[ moleculetype ]
; name         nrexcl
  MON          1

[ atoms ]
;   nr       type  resnr residue  atom   cgnr     charge       mass  typeB    chargeB      massB
; residue   1 MON rtp MON  q  0.0
     1         ho      1    MON    HO1      1      0.425      1.008   ; qtot 0.425
     2         ho      1    MON    HO2      2      0.425      1.008   ; qtot 0.85
     3         ho      1    MON    HO3      3      0.425      1.008   ; qtot 1.275
     4         ho      1    MON    HO4      4      0.425      1.008   ; qtot 1.7
     5        ohs      1    MON   OHS1      5    -1.0808         16   ; qtot 0.6192
     6        ohs      1    MON   OHS2      6    -1.0808         16   ; qtot -0.4616
     7         oh      1    MON    OH1      7      -0.95         16   ; qtot -1.412
     8         oh      1    MON    OH2      8      -0.95         16   ; qtot -2.362
     9       obos      1    MON   OBS1      9    -1.1808         16   ; qtot -3.542
    10       obos      1    MON   OBS2     10    -1.1808         16   ; qtot -4.723
    11         ob      1    MON    OB1     11      -1.05         16   ; qtot -5.773
    12       obos      1    MON   OBS3     12    -1.1808         16   ; qtot -6.954
    13       obos      1    MON   OBS4     13    -1.1808         16   ; qtot -8.135
    14         ob      1    MON    OB2     14      -1.05         16   ; qtot -9.185
    15         ob      1    MON    OB3     15      -1.05         16   ; qtot -10.23
    16         ob      1    MON    OB4     16      -1.05         16   ; qtot -11.28
    17         ob      1    MON    OB5     17      -1.05         16   ; qtot -12.33
    18         ob      1    MON    OB6     18      -1.05         16   ; qtot -13.38
    19         ob      1    MON    OB7     19      -1.05         16   ; qtot -14.43
    20         ob      1    MON    OB8     20      -1.05         16   ; qtot -15.48
    21         ob      1    MON    OB9     21      -1.05         16   ; qtot -16.53
    22         ob      1    MON   OB10     22      -1.05         16   ; qtot -17.58
    23         ob      1    MON   OB11     23      -1.05         16   ; qtot -18.63
    24         ob      1    MON   OB12     24      -1.05         16   ; qtot -19.68
    25         ob      1    MON   OB13     25      -1.05         16   ; qtot -20.73
    26         ob      1    MON   OB14     26      -1.05         16   ; qtot -21.78
    27         ob      1    MON   OB15     27      -1.05         16   ; qtot -22.83
    28         ob      1    MON   OB16     28      -1.05         16   ; qtot -23.88
    29        mgo      1    MON   MGO1     29     1.3598      24.31   ; qtot -22.52
    30         ao      1    MON    AO1     30      1.575      26.98   ; qtot -20.95
    31         ao      1    MON    AO2     31      1.575      26.98   ; qtot -19.37
    32         ao      1    MON    AO3     32      1.575      26.98   ; qtot -17.8
```

```
    33          st      1    MON     ST1     33        2.1      28.09   ; qtot -15.7
    34          st      1    MON     ST2     34        2.1      28.09   ; qtot -13.6
    35          st      1    MON     ST3     35        2.1      28.09   ; qtot -11.5
    36          st      1    MON     ST4     36        2.1      28.09   ; qtot -9.4
    37          st      1    MON     ST5     37        2.1      28.09   ; qtot -7.3
    38          st      1    MON     ST6     38        2.1      28.09   ; qtot -5.2
    39          st      1    MON     ST7     39        2.1      28.09   ; qtot -3.1
    40          st      1    MON     ST8     40        2.1      28.09   ; qtot -1

[ bonds ]
; i     j       funct   length  force.c.
1       5     1     0.1    463532.808
2       6     1        0.1    463532.808
3       7     1        0.1    463532.808
4       8     1        0.1    463532.808
```

REFERENCES

(1) Cygan, R. T.; Liang, J.-J.; Kalinichev, A. G. Molecular Models of Hydroxide, Oxyhydroxide, and Clay Phases and the Development of a General Force Field. *J. Phys. Chem. B* **2004**, *108*, 1255-1266.

(2) Berendsen, H. J. C.; Postma, J. P. M.; van Gunsteren, W. F.; Hermans, J. Interaction Models for Water in Relation to Protein Hydration. In *Intermolecular Forces*, Pullman, B., Ed. D. Reidel: 1981; pp 331- 342.

(3) Berendsen, H. J. C.; Grigera, J. R.; Straatsma, T. P. The Missing Term in Effective Pair Potentials. *J. Phys. Chem.* **1987**, *91*, 6269-6271.

(4) Teleman, O.; Jönsson, B.; Engström, S. A Molecular Dynamics Simulation of a Water Model with Intramolecular Degrees of Freedom. *Mol. Phys.* **1987**, *60*, 193-203.

(5) Greathouse, J. A.; Durkin, J. S.; Larentzos, J. P.; Cygan, R. T. Implementation of a Morse Potential to Model Hydroxyl Behavior in Phyllosilicates. *J. Chem. Phys.* **2009**, *130*, 134713.

(6) Zeitler, T. R.; Greathouse, J. A.; Gale, J. D.; Cygan, R. T. Vibrational Analysis of Brucite Surfaces and the Development of an Improved Force Field for Molecular Simulation of Interfaces. *J. Phys. Chem. C* **2014**, *118*, 7946-7953.

(7) Pouvreau, M.; Greathouse, J. A.; Cygan, R. T.; Kalinichev, A. G. Structure of Hydrated Gibbsite and Brucite Edge Surfaces: DFT Results and Further Development of the Clayff Classical Force Field with Metal-O-H Angle Bending Terms. *J. Phys. Chem. C* **2017**, *121*, 14757-14771.

(8) Pouvreau, M.; Greathouse, J. A.; Cygan, R. T.; Kalinichev, A. G. Structure of Hydrated Kaolinite Edge Structures: DFT Results and Further Development of the Clayff Classical Force Field with Metal-O-H Angle Bending Terms. *J. Phys. Chem. C* **2019**, *123*, 11628-11638.

(9) Knapp, B.; Lederer, N.; Omasits, U.; Schreiner, W. vmdICE: A Plug-in for Rapid Evaluation of Molecular Dynamics Simulations Using VMD. *J. Comput. Chem.* **2010**, *31*, 2868-2873.

(10) Stukowski, A. Visualization and Analysis of Atomistic Simulation Data with OVITO—The Open Visualization Tool. *Model. Simul. Mater. Sci. Eng.* **2010**, *18*, 015012.

(11) Jamali, S. H.; Wolff, L.; Becker, T. M.; de Groen, M.; Ramdin, M.; Hartkamp, R.; Bardow, A.; Vlugt, T. J. H.; Moultos, O. A. OCTP: A Tool for On-the-Fly Calculation of Transport Properties of Fluids with the Order-*n* Algorithm in LAMMPS. *J. Chem. Inf. Model.* **2019**, *59*, 1290-1294

(12) Holmboe, M. Atom: A Matlab Package for Manipulation of Molecular Systems. *Clays Clay Miner.* **2019**, *67*, 419-426.

(13) Åqvist, J. Ion-Water Interaction Potentials Derived from Free Energy Perturbation Simulations. *J. Phys. Chem.* **1990**, *94*, 8021-8024.

(14) Koneshan, S.; Rasaiah, J. C.; Lynden-Bell, R. M.; Lee, S. H. Solvent Structure, Dynamics, and Ion Mobility in Aqueous Solutions at 25 °C. *J. Phys. Chem. B* **1998**, *102*, 4193-4204.

(15) Li, P.; Roberts, B. P.; Chakravorty, D. K.; Merz, K. M. Rational Design of Particle Mesh Ewald Compatible Lennard-Jones Parameters for +2 Metal Cations in Explicit Solvent. *J. Chem. Theory Comput.* **2013**, *9*, 2733-2748.

(16) Li, P.; Song, L. F.; Merz, K. M. Systematic Parameterization of Monovalent Ions Employing the Nonbonded *Model. J. Chem. Theory Comput.* **2015**, 11, 1645-1657.